Selected for a Viewpoint in *Physics*
PHYSICAL REVIEW D **82,** 032001 (2010)

Evidence for an anomalous like-sign dimuon charge asymmetry

V. M. Abazov,[36] B. Abbott,[74] M. Abolins,[63] B. S. Acharya,[29] M. Adams,[49] T. Adams,[47] E. Aguilo,[6] G. D. Alexeev,[36] G. Alkhazov,[40] A. Alton,[62,*] G. Alverson,[61] G. A. Alves,[2] L. S. Ancu,[35] M. Aoki,[48] Y. Arnoud,[14] M. Arov,[58] A. Askew,[47] B. Åsman,[41] O. Atramentov,[66] C. Avila,[8] J. BackusMayes,[81] F. Badaud,[13] L. Bagby,[48] B. Baldin,[48] D. V. Bandurin,[47] S. Banerjee,[29] E. Barberis,[61] A.-F. Barfuss,[15] P. Baringer,[56] J. Barreto,[2] J. F. Bartlett,[48] U. Bassler,[18] S. Beale,[6] A. Bean,[56] M. Begalli,[3] M. Begel,[72] C. Belanger-Champagne,[41] L. Bellantoni,[48] J. A. Benitez,[63] S. B. Beri,[27] G. Bernardi,[17] R. Bernhard,[22] I. Bertram,[42] M. Besançon,[18] R. Beuselinck,[43] V. A. Bezzubov,[39] P. C. Bhat,[48] V. Bhatnagar,[27] G. Blazey,[50] S. Blessing,[47] K. Bloom,[65] A. Boehnlein,[48] D. Boline,[71] T. A. Bolton,[57] E. E. Boos,[38] G. Borissov,[42] T. Bose,[60] A. Brandt,[77] R. Brock,[63] G. Brooijmans,[69] A. Bross,[48] D. Brown,[19] X. B. Bu,[7] D. Buchholz,[51] M. Buehler,[80] V. Buescher,[24] V. Bunichev,[38] S. Burdin,[42,†] T. H. Burnett,[81] C. P. Buszello,[43] P. Calfayan,[25] B. Calpas,[15] S. Calvet,[16] E. Camacho-Pérez,[33] J. Cammin,[70] M. A. Carrasco-Lizarraga,[33] E. Carrera,[47] B. C. K. Casey,[48] H. Castilla-Valdez,[33] S. Chakrabarti,[71] D. Chakraborty,[50] K. M. Chan,[54] A. Chandra,[79] G. Chen,[56] S. Chevalier-Théry,[18] D. K. Cho,[76] S. W. Cho,[31] S. Choi,[32] B. Choudhary,[28] T. Christoudias,[43] S. Cihangir,[48] D. Claes,[65] J. Clutter,[56] M. Cooke,[48] W. E. Cooper,[48] M. Corcoran,[79] F. Couderc,[18] M.-C. Cousinou,[15] A. Croc,[18] D. Cutts,[76] M. Ćwiok,[30] A. Das,[45] G. Davies,[43] K. De,[77] S. J. de Jong,[35] E. De La Cruz-Burelo,[33] F. Déliot,[18] M. Demarteau,[48] R. Demina,[70] D. Denisov,[48] S. P. Denisov,[39] S. Desai,[48] K. DeVaughan,[65] H. T. Diehl,[48] M. Diesburg,[48] A. Dominguez,[65] T. Dorland,[81] A. Dubey,[28] L. V. Dudko,[38] D. Duggan,[66] A. Duperrin,[15] S. Dutt,[27] A. Dyshkant,[50] M. Eads,[65] D. Edmunds,[63] J. Ellison,[46] V. D. Elvira,[48] Y. Enari,[17] S. Eno,[59] H. Evans,[52] A. Evdokimov,[72] V. N. Evdokimov,[39] G. Facini,[61] A. V. Ferapontov,[76] T. Ferbel,[59,70] F. Fiedler,[24] F. Filthaut,[35] W. Fisher,[63] H. E. Fisk,[48] M. Fortner,[50] H. Fox,[42] S. Fuess,[48] T. Gadfort,[72] A. Garcia-Bellido,[70] V. Gavrilov,[37] P. Gay,[13] W. Geist,[19] W. Geng,[15,63] D. Gerbaudo,[67] C. E. Gerber,[49] Y. Gershtein,[66] D. Gillberg,[6] G. Ginther,[48,70] G. Golovanov,[36] A. Goussiou,[81] P. D. Grannis,[71] S. Greder,[19] H. Greenlee,[48] Z. D. Greenwood,[58] E. M. Gregores,[4] G. Grenier,[20] Ph. Gris,[13] J.-F. Grivaz,[16] A. Grohsjean,[18] S. Grünendahl,[48] M. W. Grünewald,[30] F. Guo,[71] J. Guo,[71] G. Gutierrez,[48] P. Gutierrez,[74] A. Haas,[69,‡] P. Haefner,[25] S. Hagopian,[47] J. Haley,[61] I. Hall,[63] L. Han,[7] K. Harder,[44] A. Harel,[70] J. M. Hauptman,[55] J. Hays,[43] T. Hebbeker,[21] D. Hedin,[50] A. P. Heinson,[46] U. Heintz,[76] C. Hensel,[23] I. Heredia-De La Cruz,[33] K. Herner,[62] G. Hesketh,[61] M. D. Hildreth,[54] R. Hirosky,[80] T. Hoang,[47] J. D. Hobbs,[71] B. Hoeneisen,[12] M. Hohlfeld,[24] S. Hossain,[74] P. Houben,[34] Y. Hu,[71] Z. Hubacek,[10] N. Huske,[17] V. Hynek,[10] I. Iashvili,[68] R. Illingworth,[48] A. S. Ito,[48] S. Jabeen,[76] M. Jaffré,[16] S. Jain,[68] D. Jamin,[15] R. Jesik,[43] K. Johns,[45] C. Johnson,[69] M. Johnson,[48] D. Johnston,[65] A. Jonckheere,[48] P. Jonsson,[43] A. Juste,[48,§] K. Kaadze,[57] E. Kajfasz,[15] D. Karmanov,[38] P. A. Kasper,[48] I. Katsanos,[65] R. Kehoe,[78] S. Kermiche,[15] N. Khalatyan,[48] A. Khanov,[75] A. Kharchilava,[68] Y. N. Kharzheev,[36] D. Khatidze,[76] M. H. Kirby,[51] M. Kirsch,[21] J. M. Kohli,[27] A. V. Kozelov,[39] J. Kraus,[63] A. Kumar,[68] A. Kupco,[11] T. Kurča,[20] V. A. Kuzmin,[38] J. Kvita,[9] S. Lammers,[52] G. Landsberg,[76] P. Lebrun,[20] H. S. Lee,[31] W. M. Lee,[48] J. Lellouch,[17] L. Li,[46] Q. Z. Li,[48] S. M. Lietti,[5] J. K. Lim,[31] D. Lincoln,[48] J. Linnemann,[63] V. V. Lipaev,[39] R. Lipton,[48] Y. Liu,[7] Z. Liu,[6] A. Lobodenko,[40] M. Lokajicek,[11] P. Love,[42] H. J. Lubatti,[81] R. Luna-Garcia,[33,‖] A. L. Lyon,[48] A. K. A. Maciel,[2] D. Mackin,[79] R. Madar,[18] R. Magaña-Villalba,[33] P. K. Mal,[45] S. Malik,[65] V. L. Malyshev,[36] Y. Maravin,[57] J. Martínez-Ortega,[33] R. McCarthy,[71] C. L. McGivern,[56] M. M. Meijer,[35] A. Melnitchouk,[64] D. Menezes,[50] P. G. Mercadante,[4] M. Merkin,[38] A. Meyer,[21] J. Meyer,[23] N. K. Mondal,[29] T. Moulik,[56] G. S. Muanza,[15] M. Mulhearn,[80] E. Nagy,[15] M. Naimuddin,[28] M. Narain,[76] R. Nayyar,[28] H. A. Neal,[62] J. P. Negret,[8] P. Neustroev,[40] H. Nilsen,[22] S. F. Novaes,[5] T. Nunnemann,[25] G. Obrant,[40] D. Onoprienko,[57] J. Orduna,[33] N. Osman,[43] J. Osta,[54] G. J. Otero y Garzón,[1] M. Owen,[44] M. Padilla,[46] M. Pangilinan,[76] N. Parashar,[53] V. Parihar,[76] S.-J. Park,[23] S. K. Park,[31] J. Parsons,[69] R. Partridge,[76,‡] N. Parua,[52] A. Patwa,[72] B. Penning,[48] M. Perfilov,[38] K. Peters,[44] Y. Peters,[44] G. Petrillo,[70] P. Pétroff,[16] R. Piegaia,[1] J. Piper,[63] M.-A. Pleier,[72] P. L. M. Podesta-Lerma,[33,¶] V. M. Podstavkov,[48] M.-E. Pol,[2] P. Polozov,[37] A. V. Popov,[39] M. Prewitt,[79] D. Price,[52] S. Protopopescu,[72] J. Qian,[62] A. Quadt,[23] B. Quinn,[64] M. S. Rangel,[16] K. Ranjan,[28] P. N. Ratoff,[42] I. Razumov,[39] P. Renkel,[78] P. Rich,[44] M. Rijssenbeek,[71] I. Ripp-Baudot,[19] F. Rizatdinova,[75] M. Rominsky,[48] C. Royon,[18] P. Rubinov,[48] R. Ruchti,[54] G. Safronov,[37] G. Sajot,[14] A. Sánchez-Hernández,[33] M. P. Sanders,[25] B. Sanghi,[48] G. Savage,[48] L. Sawyer,[58] T. Scanlon,[43] D. Schaile,[25] R. D. Schamberger,[71] Y. Scheglov,[40] H. Schellman,[51] T. Schliephake,[26] S. Schlobohm,[81] C. Schwanenberger,[44] R. Schwienhorst,[63] J. Sekaric,[56] H. Severini,[74] E. Shabalina,[23] V. Shary,[18] A. A. Shchukin,[39] R. K. Shivpuri,[28] V. Simak,[10] V. Sirotenko,[48] P. Skubic,[74] P. Slattery,[70] D. Smirnov,[54] G. R. Snow,[65] J. Snow,[73] S. Snyder,[72] S. Söldner-Rembold,[44] L. Sonnenschein,[21] A. Sopczak,[42] M. Sosebee,[77] K. Soustruznik,[9] B. Spurlock,[77] J. Stark,[14] V. Stolin,[37] D. A. Stoyanova,[39] M. A. Strang,[68] E. Strauss,[71] M. Strauss,[74] R. Ströhmer,[25] D. Strom,[49] L. Stutte,[48] P. Svoisky,[35] M. Takahashi,[44] A. Tanasijczuk,[1] W. Taylor,[6] B. Tiller,[25] M. Titov,[18] V. V. Tokmenin,[36] D. Tsybychev,[71]

B. Tuchming,[18] C. Tully,[67] P. M. Tuts,[69] R. Unalan,[63] L. Uvarov,[40] S. Uvarov,[40] S. Uzunyan,[50] R. Van Kooten,[52] W. M. van Leeuwen,[34] N. Varelas,[49] E. W. Varnes,[45] I. A. Vasilyev,[39] P. Verdier,[20] L. S. Vertogradov,[36] M. Verzocchi,[48] M. Vesterinen,[44] D. Vilanova,[18] P. Vint,[43] P. Vokac,[10] H. D. Wahl,[47] M. H. L. S. Wang,[70] J. Warchol,[54] G. Watts,[81] M. Wayne,[54] G. Weber,[24] M. Weber,[48,**] M. Wetstein,[59] A. White,[77] D. Wicke,[24] M. R. J. Williams,[42] G. W. Wilson,[56] S. J. Wimpenny,[46] M. Wobisch,[58] D. R. Wood,[61] T. R. Wyatt,[44] Y. Xie,[48] C. Xu,[62] S. Yacoob,[51] R. Yamada,[48] W.-C. Yang,[44] T. Yasuda,[48] Y. A. Yatsunenko,[36] Z. Ye,[48] H. Yin,[7] K. Yip,[72] H. D. Yoo,[76] S. W. Youn,[48] J. Yu,[77] S. Zelitch,[80] T. Zhao,[81] B. Zhou,[62] J. Zhu,[71] M. Zielinski,[70] D. Zieminska,[52] and L. Zivkovic[69]

(D0 Collaboration)

[1]*Universidad de Buenos Aires, Buenos Aires, Argentina*
[2]*LAFEX, Centro Brasileiro de Pesquisas Físicas, Rio de Janeiro, Brazil*
[3]*Universidade do Estado do Rio de Janeiro, Rio de Janeiro, Brazil*
[4]*Universidade Federal do ABC, Santo André, Brazil*
[5]*Instituto de Física Teórica, Universidade Estadual Paulista, São Paulo, Brazil*
[6]*Simon Fraser University, Vancouver, British Columbia, Canada and York University, Toronto, Ontario, Canada*
[7]*University of Science and Technology of China, Hefei, People's Republic of China*
[8]*Universidad de los Andes, Bogotá, Colombia*
[9]*Charles University, Faculty of Mathematics and Physics, Center for Particle Physics, Prague, Czech Republic*
[10]*Czech Technical University in Prague, Prague, Czech Republic*
[11]*Center for Particle Physics, Institute of Physics, Academy of Sciences of the Czech Republic, Prague, Czech Republic*
[12]*Universidad San Francisco de Quito, Quito, Ecuador*
[13]*LPC, Université Blaise Pascal, CNRS/IN2P3, Clermont, France*
[14]*LPSC, Université Joseph Fourier Grenoble 1, CNRS/IN2P3, Institut National Polytechnique de Grenoble, Grenoble, France*
[15]*CPPM, Aix-Marseille Université, CNRS/IN2P3, Marseille, France*
[16]*LAL, Université Paris-Sud, CNRS/IN2P3, Orsay, France*
[17]*LPNHE, Universités Paris VI and VII, CNRS/IN2P3, Paris, France*
[18]*CEA, Irfu, SPP, Saclay, France*
[19]*IPHC, Université de Strasbourg, CNRS/IN2P3, Strasbourg, France*
[20]*IPNL, Université Lyon 1, CNRS/IN2P3, Villeurbanne, France and Université de Lyon, Lyon, France*
[21]*III. Physikalisches Institut A, RWTH Aachen University, Aachen, Germany*
[22]*Physikalisches Institut, Universität Freiburg, Freiburg, Germany*
[23]*II. Physikalisches Institut, Georg-August-Universität Göttingen, Göttingen, Germany*
[24]*Institut für Physik, Universität Mainz, Mainz, Germany*
[25]*Ludwig-Maximilians-Universität München, München, Germany*
[26]*Fachbereich Physik, Bergische Universität Wuppertal, Wuppertal, Germany*
[27]*Panjab University, Chandigarh, India*
[28]*Delhi University, Delhi, India*
[29]*Tata Institute of Fundamental Research, Mumbai, India*
[30]*University College Dublin, Dublin, Ireland*
[31]*Korea Detector Laboratory, Korea University, Seoul, Korea*
[32]*SungKyunKwan University, Suwon, Korea*
[33]*CINVESTAV, Mexico City, Mexico*
[34]*FOM-Institute NIKHEF and University of Amsterdam/NIKHEF, Amsterdam, The Netherlands*
[35]*Radboud University Nijmegen/NIKHEF, Nijmegen, The Netherlands*
[36]*Joint Institute for Nuclear Research, Dubna, Russia*
[37]*Institute for Theoretical and Experimental Physics, Moscow, Russia*
[38]*Moscow State University, Moscow, Russia*
[39]*Institute for High Energy Physics, Protvino, Russia*
[40]*Petersburg Nuclear Physics Institute, St. Petersburg, Russia*
[41]*Stockholm University, Stockholm, Sweden and Uppsala University, Uppsala, Sweden*
[42]*Lancaster University, Lancaster LA1 4YB, United Kingdom*
[43]*Imperial College London, London SW7 2AZ, United Kingdom*
[44]*The University of Manchester, Manchester M13 9PL, United Kingdom*
[45]*University of Arizona, Tucson, Arizona 85721, USA*
[46]*University of California Riverside, Riverside, California 92521, USA*
[47]*Florida State University, Tallahassee, Florida 32306, USA*
[48]*Fermi National Accelerator Laboratory, Batavia, Illinois 60510, USA*
[49]*University of Illinois at Chicago, Chicago, Illinois 60607, USA*

[50]Northern Illinois University, DeKalb, Illinois 60115, USA
[51]Northwestern University, Evanston, Illinois 60208, USA
[52]Indiana University, Bloomington, Indiana 47405, USA
[53]Purdue University Calumet, Hammond, Indiana 46323, USA
[54]University of Notre Dame, Notre Dame, Indiana 46556, USA
[55]Iowa State University, Ames, Iowa 50011, USA
[56]University of Kansas, Lawrence, Kansas 66045, USA
[57]Kansas State University, Manhattan, Kansas 66506, USA
[58]Louisiana Tech University, Ruston, Louisiana 71272, USA
[59]University of Maryland, College Park, Maryland 20742, USA
[60]Boston University, Boston, Massachusetts 02215, USA
[61]Northeastern University, Boston, Massachusetts 02115, USA
[62]University of Michigan, Ann Arbor, Michigan 48109, USA
[63]Michigan State University, East Lansing, Michigan 48824, USA
[64]University of Mississippi, University, Mississippi 38677, USA
[65]University of Nebraska, Lincoln, Nebraska 68588, USA
[66]Rutgers University, Piscataway, New Jersey 08855, USA
[67]Princeton University, Princeton, New Jersey 08544, USA
[68]State University of New York, Buffalo, New York 14260, USA
[69]Columbia University, New York, New York 10027, USA
[70]University of Rochester, Rochester, New York 14627, USA
[71]State University of New York, Stony Brook, New York 11794, USA
[72]Brookhaven National Laboratory, Upton, New York 11973, USA
[73]Langston University, Langston, Oklahoma 73050, USA
[74]University of Oklahoma, Norman, Oklahoma 73019, USA
[75]Oklahoma State University, Stillwater, Oklahoma 74078, USA
[76]Brown University, Providence, Rhode Island 02912, USA
[77]University of Texas, Arlington, Texas 76019, USA
[78]Southern Methodist University, Dallas, Texas 75275, USA
[79]Rice University, Houston, Texas 77005, USA
[80]University of Virginia, Charlottesville, Virginia 22901, USA
[81]University of Washington, Seattle, Washington 98195, USA

(Received 16 May 2010; published 16 August 2010)

We measure the charge asymmetry A of like-sign dimuon events in 6.1 fb^{-1} of $p\bar{p}$ collisions recorded with the D0 detector at a center-of-mass energy $\sqrt{s} = 1.96$ TeV at the Fermilab Tevatron collider. From A, we extract the like-sign dimuon charge asymmetry in semileptonic b-hadron decays: $A^b_{\rm sl} = -0.00957 \pm 0.00251\ (\text{stat}) \pm 0.00146\ (\text{syst})$. This result differs by 3.2 standard deviations from the standard model prediction $A^b_{\rm sl}(\text{SM}) = (-2.3^{+0.5}_{-0.6}) \times 10^{-4}$ and provides first evidence of anomalous CP violation in the mixing of neutral B mesons.

DOI: 10.1103/PhysRevD.82.032001 PACS numbers: 13.25.Hw, 11.30.Er, 14.40.Nd

I. INTRODUCTION

Studies of particle production and decay under the reversal of discrete symmetries (charge, parity, and time reversal) have yielded considerable insight on the structure of the theories that describe high energy phenomena. Of particular interest is the observation of CP violation, a phenomenon well established in the K^0 and B^0_d systems, but not yet observed for the B^0_s system, where all CP violation effects are expected to be small in the standard model (SM) [1]. (See [2] and references therein for a review of the experimental results and of the theoretical framework for describing CP violation in neutral meson decays.) The violation of CP symmetry is a necessary condition for baryogenesis, the process thought to be responsible for the matter-antimatter asymmetry of the Universe [3]. However, the observed CP violation in the K^0 and B^0_d systems, consistent with the standard model expectation, is not sufficient to explain this asymmetry, suggesting the presence of additional sources of CP violation, beyond the standard model [4].

The D0 experiment at the Fermilab Tevatron proton-antiproton ($p\bar{p}$) collider, operating at a center-of-mass

*Visitor from Augustana College, Sioux Falls, SD, USA.
†Visitor from The University of Liverpool, Liverpool, UK.
‡Visitor from SLAC, Menlo Park, CA, USA.
§Visitor from ICREA/IFAE, Barcelona, Spain.
‖Visitor from Centro de Investigacion en Computacion - IPN, Mexico City, Mexico.
¶Visitor from ECFM, Universidad Autonoma de Sinaloa, Culiacán, Mexico.
**Visitor from Universität Bern, Bern, Switzerland.

energy $\sqrt{s} = 1.96$ TeV, is in a unique position to study possible effects of CP violation, in particular, through the study of charge asymmetries in generic final states, given that the initial state is CP symmetric. The high center-of-mass energy provides access to mass states beyond the reach of the B factories. The periodic reversal of the D0 solenoid and toroid polarities results in a cancellation at the first order of most detector-related asymmetries. In this paper we present a measurement of the like-sign dimuon charge asymmetry A, defined as

$$A \equiv \frac{N^{++} - N^{--}}{N^{++} + N^{--}}, \tag{1}$$

where N^{++} and N^{--} represent, respectively, the number of events in which the two muons of highest transverse momentum satisfying the kinematic selections have the same positive or negative charge. After removing the contributions from backgrounds and from residual detector effects, we observe a net asymmetry that is significantly different from zero.

We interpret this result assuming that the only source of this asymmetry is the mixing of neutral B mesons that decay semileptonically, and obtain a measurement of the asymmetry $A^b_{\rm sl}$ defined as

$$A^b_{\rm sl} \equiv \frac{N^{++}_b - N^{--}_b}{N^{++}_b + N^{--}_b}, \tag{2}$$

where N^{++}_b and N^{--}_b represent the number of events containing two b hadrons decaying semileptonically and producing two positive or two negative muons, respectively. As shown in Appendix A each neutral B^0_q meson ($q = d, s$) contributes a term to this asymmetry given by

$$a^q_{\rm sl} = \frac{\Delta\Gamma_q}{\Delta M_q}\tan\phi_q, \tag{3}$$

where ϕ_q is the CP-violating phase, and ΔM_q and $\Delta\Gamma_q$ are the mass and width differences between the eigenstates of the mass matrices of the neutral B^0_q mesons. The SM predicts the values $\phi_s = 0.0042 \pm 0.0014$ and $\phi_d = -0.091^{+0.026}_{-0.038}$ [1]. These values set the scale for the expected asymmetries in the semileptonic decays of B^0_q mesons that are negligible compared to the present experimental sensitivity [1]. In the standard model $A^b_{\rm sl}$ is

$$A^b_{\rm sl}({\rm SM}) = (-2.3^{+0.5}_{-0.6}) \times 10^{-4}, \tag{4}$$

where the uncertainty is mainly due to experimental measurement of the fraction of B^0_q mesons produced in $p\bar{p}$ collisions at the Tevatron, and of the parameters controlling the mixing of neutral B mesons. The B^0_d semileptonic charge asymmetry, which constrains the phase ϕ_d, has been measured at e^+e^- colliders [2], and the most precise results reported by the *BABAR* and Belle Collaborations, given in Refs. [5,6], are in agreement with the SM prediction. Extensions of the SM could produce additional contributions to the Feynman box diagrams responsible for B^0_q mixing and other corrections that can provide larger values of ϕ_q [7–11]. Measurements of $A^b_{\rm sl}$ or ϕ_q that differ significantly from the SM expectations would indicate the presence of new physics.

The asymmetry $A^b_{\rm sl}$ is also equal to the charge asymmetry $a^b_{\rm sl}$ of semileptonic decays of b hadrons to muons of "wrong charge" (i.e. a muon charge opposite to the charge of the original b quark) induced through $B^0_q\bar{B}^0_q$ oscillations [12]:

$$a^b_{\rm sl} \equiv \frac{\Gamma(\bar{B} \to \mu^+X) - \Gamma(B \to \mu^-X)}{\Gamma(\bar{B} \to \mu^+X) + \Gamma(B \to \mu^-X)} = A^b_{\rm sl}. \tag{5}$$

We extract $A^b_{\rm sl}$ from two observables. The first is the like-sign dimuon charge asymmetry A of Eq. (1), and the second observable is the inclusive muon charge asymmetry a defined as

$$a \equiv \frac{n^+ - n^-}{n^+ + n^-}, \tag{6}$$

where n^+ and n^- correspond to the number of detected positive and negative muons, respectively.

At the Fermilab Tevatron collider, b quarks are produced mainly in $b\bar{b}$ pairs. The signal for the asymmetry A is composed of like-sign dimuon events, with one muon arising from direct semileptonic b-hadron decay $b \to \mu^-X$ [13], and the other muon resulting from $B^0_q\bar{B}^0_q$ oscillation, followed by the direct semileptonic $\bar{B}^0_q$-meson decay $B^0_q \to \bar{B}^0_q \to \mu^-X$. Consequently the second muon has the "wrong sign" due to $B^0_q\bar{B}^0_q$ mixing. For the asymmetry a, the signal comes from mixing, followed by the semileptonic decay $B^0_q \to \bar{B}^0_q \to \mu^-X$. The main backgrounds for these measurements arise from events with at least one muon from kaon or pion decay, or from the sequential decay of b quarks $b \to c \to \mu^+X$. For the asymmetry a, there is an additional background from direct production of c quarks followed by their semileptonic decays.

The data used in this analysis were recorded with the D0 detector [14–16] at the Fermilab Tevatron proton-antiproton collider between April 2002 and June 2009 and correspond to an integrated luminosity of 6.1 ± 0.4 fb^{-1}. The result presented in this article supersedes our previous measurement [17] based on the initial data set corresponding to 1 fb^{-1} of integrated luminosity. In addition to the larger data set, the main difference between these two analyses is that almost all quantities in the present measurement are obtained directly from data, with minimal input from simulation. To avoid any bias, the central value of the asymmetry was extracted from the full data set only after all other aspects of the analysis and all systematic uncertainties had been finalized.

The outline of the paper is as follows. In Sec. II, we present the strategy of the measurement. The detector and data selections are discussed in Sec. III, and in Sec. IV we

describe the Monte Carlo (MC) simulations used in this analysis. Sections V, VI, VII, VIII, IX, X, XI, XII, and XIII provide further details. Section XIV presents the results, Sec. XV describes consistency checks, Sec. XVI compares the obtained result with other existing measurements, and, finally, Sec. XVII gives the conclusions. Appendixes A, B, C, D, and E provide additional technical details on aspects of the analysis.

II. MEASUREMENT METHOD

We measure the dimuon charge asymmetry A defined in Eq. (1) and the inclusive muon charge asymmetry a of Eq. (6), starting from a dimuon data sample and an inclusive muon sample, respectively. Background processes and detector asymmetries contribute to these asymmetries. These contributions are measured directly in data and used to correct the asymmetries. After applying these corrections, the only expected source of residual asymmetry in both the inclusive muon and dimuon samples is from the asymmetry $A^b_{\rm sl}$. Simulations are used to relate the residual asymmetries to the asymmetry $A^b_{\rm sl}$, and to obtain two independent measurements of $A^b_{\rm sl}$. These measurements are combined to take advantage of the correlated contributions from backgrounds, and to reduce the total uncertainties in the determination of $A^b_{\rm sl}$.

The source of the asymmetry a has its nominal origin in the semileptonic charge asymmetry of neutral B mesons, defined in Eq. (5). However, various detector and material-related processes also contribute to $n^{\pm}$. We classify all muons into two categories according to their origin. The first category, ''short,'' denoted in the following as S, includes muons from weak decays of b and c quarks and τ leptons, and from electromagnetic decays of the short-lived mesons ($\phi, \omega, \eta, \rho^0$). The muons in the second, ''long,'' category denoted as L, come from decays of charged kaons and pions and from other processes: charged kaons, pions, and protons not fully absorbed by the calorimeter and reaching the muon detectors (''punchthrough''), and false matches of central tracks produced by kaons, pions, or protons to a track segment reconstructed in the muon detector. Thus, the L sample contains only the contribution from long-lived particles. The total number of muons in the inclusive muon sample is

$$n = n^+ + n^- = n_S + n_L, \tag{7}$$

where n_S is the number of S muons, and n_L is the number of L muons.

The initial number of observed μ^+ (upper signs) or μ^- (lower signs) is

$$n^{\pm} \propto f_S(1 \pm a_S)(1 \pm \delta) + f_K(1 \pm a_K) + f_\pi(1 \pm a_\pi) + f_p(1 \pm a_p). \tag{8}$$

In this expression, the quantity δ is the charge asymmetry related to muon detection and identification, f_K is the fraction of muons from charged kaon decay, punchthrough, or false association with a kaon track, and a_K is their charge asymmetry. This asymmetry is measured directly in data as described in Sec. XI, and therefore, by definition, includes the contribution from δ. The analogous quantities f_π and f_p represent the fraction of muons from charged pion decay, punchthrough or false muon association with a pion track, and proton punchthrough or false muon association with a proton track, respectively, while a_π and a_p represent the corresponding charge asymmetries. The fraction f_p also includes a contribution from the association of falsely identified tracks with muons. The quantity $f_{\rm bkg} \equiv n_L/(n_S + n_L) = f_K + f_\pi + f_p$ is the L background fraction, $f_S \equiv n_S/(n_S + n_L) = 1 - f_{\rm bkg}$ is the fraction of S muons, and a_S is related to the semileptonic charge asymmetry $A^b_{\rm sl}$, as discussed in Sec. XIII. The charge asymmetry a can be expressed in terms of these quantities as

$$a = f_S a_S + a_{\rm bkg}, \tag{9}$$

$$a_{\rm bkg} \equiv f_s\delta + f_K a_K + f_\pi a_\pi + f_p a_p, \tag{10}$$

where, because of the small values of δ and a_S, only terms that depend linearly on the asymmetries are considered.

The most important background term is $f_K a_K$, which measures the contribution from kaon decay and punchthrough. The asymmetry a_K reflects the fact that the inelastic interaction length of the K^+ meson is greater than that of the K^- meson [2]. This difference arises from additional hyperon production channels in K^--nucleon reactions, which are absent for their K^+-nucleon analogs. Since the interaction probability of K^+ mesons is smaller, they travel farther than K^- in the detector material, and have a greater chance of decaying to muons, and a larger probability to punchthrough the absorber material thereby mimicking a muon signal. As a result, the asymmetry a_K is positive. Since all other asymmetries are at least a factor of 10 smaller than a_K, neglecting the quadratic terms in Eq. (9) produces an impact of $<1\%$ on the final result.

In analogy with Eq. (7), the number of like-sign dimuon events can be written as

$$N = N^{++} + N^{--} = N_{SS} + N_{SL} + N_{LL}, \tag{11}$$

where N_{SS} (N_{LL}) is the number of like-sign dimuon events with two S (L) muons, and, similarly, N_{SL} is the number of events with one S and one L muon. A particle producing an L muon can be a kaon, pion, or proton, and, correspondingly, we define the numbers N^x_{SL} with $x = K, \pi$, and p. In a similar way, we define N^{xy}_{LL} with $x, y = K, \pi$, and p. The corresponding fractions, defined per like-sign dimuon event, are $F^x_{SL} \equiv N^x_{SL}/N$ and $F^{xy}_{LL} \equiv N^{xy}_{LL}/N$. We also define $F_{SS} \equiv N_{SS}/N$, $F_{SL} \equiv N_{SL}/N$, and $F_{LL} \equiv N_{LL}/N$.

The number of observed like-sign dimuon events $\mu^+\mu^+$ (upper signs) or $\mu^-\mu^-$ (lower signs) is

$$N^{\pm\pm} \propto F_{SS}(1 \pm A_S)(1 \pm \Delta)^2 + \sum_{x=K,\pi,p} F_{SL}^{x}(1 \pm A_x)(1 \pm a_S)(1 \pm \Delta) + \sum_{x,y=K,\pi,} \sum_{p;y\geq x} F_{LL}^{xy}(1 \pm A_x)(1 \pm A_y). \quad (12)$$

The charge asymmetry of N_{SS} events contains the contribution from the expected asymmetry A_S that we want to measure, and the charge asymmetry Δ related to the detection and identification of muons. The asymmetry of the N_{SL} events contains the contribution of background asymmetries A_x ($x = K, \pi, p$) for one muon, and the asymmetry $(1 \pm a_S)(1 \pm \Delta)$ for the other muon. The asymmetry of N_{LL} events contains the contribution from background asymmetries A_x for both muons. By definition, the detection asymmetry Δ is included in the values of A_K, A_π, and A_p.

Keeping only the terms linear in asymmetries, the uncorrected dimuon charge asymmetry defined in Eq. (1) can be expressed as

$$A \equiv \frac{N^{++} - N^{--}}{N^{++} + N^{--}} = F_{SS}A_S + F_{SL}a_S + A_{\text{bkg}}, \quad (13)$$

$$A_{\text{bkg}} \equiv (2 - F_{\text{bkg}})\Delta + F_K A_K + F_\pi A_\pi + F_p A_p, \quad (14)$$

where $F_K = F_{SL}^{K} + F_{LL}^{K\pi} + F_{LL}^{Kp} + 2F_{LL}^{KK}$ is the total number of muons from charged kaon decay or punchthrough per like-sign dimuon event, and the quantities F_π and F_p are defined similarly for charged pions and protons. The background fraction F_{bkg} is

$$F_{\text{bkg}} \equiv F_K + F_\pi + F_p = F_{SL} + 2F_{LL}. \quad (15)$$

From Eqs. (11) and (15), it follows that

$$F_{SS} + F_{\text{bkg}} - F_{LL} = 1. \quad (16)$$

As in Eq. (9), the largest background contribution in Eq. (13) is from the term $F_K A_K$, and all other terms are found to be at least a factor of 10 smaller. The estimated contribution from the neglected quadratic terms in Eq. (13) is $\approx 2 \times 10^{-5}$, which corresponds to $\approx 4\%$ of the statistical uncertainty on A.

In the following sections, we determine from data all the parameters in Eqs. (9) and (13) used to relate the measured uncorrected asymmetries a and A to the asymmetries a_S and A_S. The detection charge asymmetry Δ can differ from δ due to differences in the muon transverse momentum p_T and pseudorapidity η [18] distributions of the like-sign dimuon and inclusive muon data samples. On physics grounds we expect the asymmetries a_x and A_x to be identical for any particle of given p_T and η. The fractions f_x in Eq. (9) and F_x in Eq. (13) for $x = K$, π, and p may be different due to the different composition of the inclusive muon and like-sign dimuon samples. For example, the inclusive muon sample contains a contribution of charm production followed by $c \to \mu X$ decay, and the like-sign dimuon sample does not. The muons in these samples also have different p_T and η distributions.

All measurements are performed as a function of the muon p_T measured in the central tracker. The range of p_T values between 1.5 and 25 GeV is divided into five bins, as shown in Table I. The term $f_K a_K$ is obtained by the weighted average of the measured values of $f_K^i a_K^i$, $i = 0$, 1, 2, 3, 4, with weights given by the fraction of muons in a given p_T interval, f_μ^i, in the inclusive muon sample:

$$f_K a_K = \sum_{i=0}^{4} f_\mu^i f_K^i a_K^i. \quad (17)$$

Similarly, the term $F_K A_K$ is computed as

$$F_K A_K = \sum_{i=0}^{4} F_\mu^i F_K^i a_K^i, \quad (18)$$

where F_μ^i is the fraction of muons in a given p_T interval in the like-sign dimuon sample. Since the kaon asymmetry is determined by the properties of the particle and not those of the event, we use the same asymmetry a_K^i for a given p_T interval in both the inclusive muon and the like-sign dimuon sample. We verify in Sec. XV that the final result does not depend significantly on muon η, nor upon kinematic properties of events, luminosity, or the mass of the $\mu\mu$ system. The definition of the muon p_T intervals and the values of f_μ^i and F_μ^i are given in Table I. The same procedure is applied to all other terms in Eqs. (9) and (13), e.g.,

$$(2 - F_{\text{bkg}})\Delta = \sum_{i=0}^{4} F_\mu^i (2 - F_{\text{bkg}}^i)\delta_i. \quad (19)$$

As in the case of a_S, the source of the asymmetry A_S is the charge asymmetry in semileptonic B-meson decays. Thus, two independent measurements of A_{sl}^b can be performed using the inclusive muon and like-sign dimuon data samples. The asymmetry a_S is dominated by detector effects, mostly due to the asymmetry arising from the different interaction lengths of charged kaons. However, A_S is far more sensitive to the asymmetry A_{sl}^b because of the definition of A in Eq. (1), which has the number of like-sign dimuon events, rather than all dimuon events in the de-

TABLE I. Fractions of muon candidates in the inclusive muon (f_μ^i) and in the like-sign dimuon (F_μ^i, with two entries per event) samples.

Bin	Muon p_T range (GeV)	f_μ^i	F_μ^i
0	1.5–2.5	0.0055	0.0442
1	2.5–4.2	0.1636	0.2734
2	4.2–7.0	0.6587	0.5017
3	7.0–10.0	0.1175	0.1238
4	10.0–25.0	0.0547	0.0569

nominator. Although a weighted average of these $A_{\rm sl}^b$ measurements can be made, we take advantage of correlations among backgrounds and asymmetries to further improve the precision of $A_{\rm sl}^b$ through a linear combination of A and a. In this combination, which is discussed in Sec. XIV, the detector effects and related systematic uncertainties cancel to a large degree, resulting in an improved measurement of $A_{\rm sl}^b$.

III. DETECTOR AND DATA SELECTION

The D0 detector is described in Refs. [14–16]. It consists of a magnetic central-tracking system that comprises a silicon microstrip tracker (SMT) and a central fiber tracker (CFT), both located within a 1.9 T superconducting solenoidal magnet [15]. The SMT has $\approx 800\,000$ individual strips, with a typical pitch of 50–80 μm, and a design optimized for tracking and vertexing for $|\eta| < 2.5$. The system has a six-barrel longitudinal structure, each with a set of four layers arranged axially around the beam pipe, and interspersed with 16 radial disks. In the spring of 2006, a "layer 0" barrel detector with 12 288 additional strips was installed [16], and two radial disks were removed. The sensors of layer 0 are located at a radius of 17 mm from the colliding beams. The CFT has eight thin coaxial barrels, each supporting two doublets of overlapping scintillating fibers of 0.835 mm diameter, one doublet parallel to the collision axis, and the other alternating by $\pm 3^\circ$ relative to the axis. Light signals are transferred via clear fibers to visual light photon counters that have $\approx 80\%$ quantum efficiency.

The muon system [14] is located beyond the liquid argon-uranium calorimeters that surround the central-tracking system, and consists of a layer A of tracking detectors and scintillation trigger counters before 1.8 T iron toroids, followed by two similar layers B and C after the toroids. Tracking for $|\eta| < 1$ relies on 10-cm wide drift tubes, while 1-cm minidrift tubes are used for $1 < |\eta| < 2$.

The trigger and data acquisition systems are designed to handle the high instantaneous luminosities. Based on information from tracking, calorimetry, and muon systems, the output of the first level of the trigger is used to limit the rate for accepted events to <2 kHz. At the next trigger stage, with more refined information, the rate is reduced further to <1 kHz. These first two levels of triggering rely mainly on hardware and firmware. The third and final level of the trigger, with access to full event information, uses software algorithms and a computing farm, and reduces the output rate to <200 Hz, which is written to tape.

The single muon and dimuon triggers used in this analysis are based on the information provided by the muon detectors, combined with the tracks reconstructed by the tracking system. The single muon triggers with the lowest p_T threshold are prescaled at high instantaneous luminosity, have a higher average p_T threshold than the dimuon triggers, and cover a smaller range of pseudorapidity than the dimuon triggers.

In this analysis we select events with one or two muons. We therefore first apply track selections, and then require either one or two muons.

Track selection: We select tracks with p_T in the range $1.5 < p_T < 25$ GeV and $|\eta| < 2.2$. The upper limit on the transverse momentum is applied to suppress the contribution of muons from W and Z boson decays. To ensure that the muon candidate can pass through the detector, including all three layers of the muon system, we require either $p_T > 4.2$ GeV or a longitudinal momentum component $|p_z| > 6.4$ GeV. The selected tracks have to satisfy the following quality requirements: at least 2 axial and 1 stereo hits in the SMT, and at least 3 axial and 3 stereo hits in the CFT. The primary interaction vertex closest to this track must contain at least five charged particles. This vertex is determined for each event using all reconstructed tracks. The average position of the collision point in the plane transverse to the beam is measured for each run and is used as a constraint. The precision of the primary vertex reconstruction for each event is on average ≈ 20 μm in the transverse plane and ≈ 40 μm along the beam direction. The transverse impact parameter of the selected track relative to the closest primary vertex must be <0.3 cm, with the longitudinal distance from the point of closest approach to this vertex <0.5 cm.

Single muon selection: The selected track must have a matching track segment reconstructed in the muon system, with at least two hits in the layer A chambers, at least two hits in the layer B or C chambers, and at least one scintillator hit associated with the track. The χ^2 for the difference between the track parameters measured in the central tracker and in the muon system must be less than 40 (with 5 d.o.f.); the measured time in at least one of the scintillators associated with the muon candidate must be within 5 ns of the expected time. The muon is assigned the charge of the track reconstructed in the central tracker. For muon $p_T < 25$ GeV, the fraction of muons with mismeasured charge and their contribution to the asymmetries are found to be negligible. The scintillator timing and the track impact parameter requirements reduce the background from cosmic rays and from beam halo to a negligible level.

Dimuon selection: The two highest transverse momentum muons in the event must pass all the selections described above, and be associated with the same interaction vertex, applying the same requirements on the transverse impact parameter and on the distance of closest approach to the primary vertex along the beam axis used in the single muon selection. To remove events in which the two muons originate from the decay of the same b hadron, we require that the invariant mass of the two muons be >2.8 GeV.

These requirements define the *reference selections*, which are changed while performing consistency checks of the analysis. Unless stated otherwise all figures, tables, and results in this article refer to these reference selections.

TABLE II. Weights assigned to the events with different solenoid and toroid polarities in the inclusive muon and like-sign dimuon samples.

Solenoid polarity	Toroid polarity	Weight inclusive muon	Weight like-sign dimuon
−1	−1	0.895	0.879
−1	+1	1.000	1.000
+1	−1	0.954	0.961
+1	+1	0.939	0.955

This analysis uses two data samples. The *inclusive* muon sample contains all events with at least one muon candidate passing the muon selection and at least one single muon trigger. If an event contains more than one muon, each muon is included in the inclusive muon sample. Such events constitute about 0.5% of the total inclusive muon sample. The *like-sign* dimuon sample contains all events with at least two muon candidates of the same charge that pass the reference dimuon selection and at least one dimuon trigger. If more than two muons pass the single muon selection, the two muons with the highest p_T are selected for inclusion in the dimuon sample. Such events comprise $\approx 0.7\%$ of the total like-sign dimuon sample.

The polarities of the toroidal and solenoidal magnetic fields are reversed on average every two weeks so that the four solenoid-toroid polarity combinations are exposed to approximately the same integrated luminosity. This allows for a cancellation of first order effects related to the instrumental asymmetry [17]. In particular, it is shown in [17] that the detector-related asymmetry denoted in [17] as $A_{\alpha\beta}$ is $\approx 0.7\%$. The contribution of this asymmetry changes sign with reversal of the toroid polarity. Therefore, it cancels after averaging over the magnet polarities, and the residual detector asymmetry measured in Sec. X is found to be less than 0.1%. To ensure such cancellation, the events are weighted according to the integrated luminosity for each data set corresponding to a different configuration of the magnets' polarities. These weights are given in Table II.

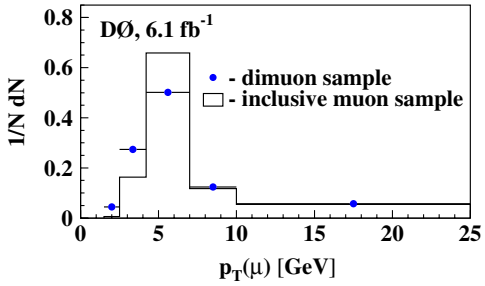

FIG. 1 (color online). The normalized muon p_T distribution. The points correspond to the like-sign dimuon sample and the histogram corresponds to the inclusive muon sample. The distribution for the like-sign dimuon sample contains two entries per event.

The normalized p_T distributions of muons in the selected data samples are shown in Fig. 1. Differences in these distributions are caused by the trigger requirements.

IV. MONTE CARLO SIMULATION

Since almost all quantities are extracted from data, the MC simulations are used in only a limited way. The simulations of QCD processes used in this analysis are as follows:

(i) Inclusive $p\bar{p}$ collisions containing a minimum transverse energy $E_T^{\min} > 10$ or 20 GeV at the generator level.

(ii) Inclusive $p\bar{p} \to b\bar{b}X$ and $p\bar{p} \to c\bar{c}X$ final states containing a muon, with an additional requirement that the b or c quark has transverse momentum $p_T > 3$ GeV, and that the produced muon has $p_T > 1.5$ GeV and $|\eta| < 2.1$.

The samples with different $E_T^{\min}$ are used to study the impact of the kinematics of generated events on the parameters extracted from the simulation.

In all cases we use the PYTHIA V6.409 [19] event generator, interfaced to the EVTGEN decay package [20] and the CTEQ6L1 [21] parton distribution functions. The generated events are propagated through the D0 detector using a GEANT [22] based program with full detector simulation. The response in the detector is digitized, and the effects of multiple interactions at high luminosity are modeled by overlaying hits from randomly triggered $p\bar{p}$ collisions on the digitized hits from MC simulation. The complete events are reconstructed with the same program as used for data, and, finally, analyzed using the same selection criteria described above for data.

V. MEASUREMENT OF f_K, F_K

A kaon, pion, or proton can be misidentified as a muon and thus contribute to the inclusive muon and the like-sign dimuon samples. This can happen because of pion and kaon decays in flight, punchthrough, or muon misidentification. We do not distinguish these individual processes, but rather measure the total fraction of such particles using data. In the following, the notation $K \to \mu$ stands for the phrase "kaon misidentified as a muon," and the notations $\pi \to \mu$ and $p \to \mu$ have corresponding meanings for pions and protons. In this section we discuss the measurement of f_K and F_K. The measurements of the corresponding factors for pions and protons and of the asymmetries are discussed in the following sections.

The fraction f_K in the inclusive muon sample is measured using $K^{*0} \to K^+\pi^-$ decays [13] with $K \to \mu$. The fraction $f_{K^{*0}}$ of these decays is related to the fraction f_K by

$$f_{K^{*0}} = \varepsilon_0 f_K R(K^{*0}), \tag{20}$$

where $R(K^{*0})$ is the fraction of all kaons that result from $K^{*0} \to K^+\pi^-$ decays, and ε_0 is the efficiency to recon-

struct the pion from the $K^{*0} \to K^+\pi^-$ decay, provided that the $K \to \mu$ track is reconstructed.

We also select K_S mesons and reconstruct $K^{*+} \to K_S\pi^+$ decays. The number of these decays is

$$N(K^{*+} \to K_S\pi^+) = \varepsilon_c N(K_S) R(K^{*+}), \quad (21)$$

where $R(K^{*+})$ is the fraction of K_S that result from $K^{*+} \to K_S\pi^+$ decays, and ε_c is the efficiency to reconstruct the additional pion in the $K^{*+} \to K_S\pi^+$ decay, provided that the K_S meson is reconstructed. We use isospin invariance to set

$$R(K^{*0}) = R(K^{*+}). \quad (22)$$

This relation is also confirmed by data as discussed in Sec. VIII. We apply the same kinematic selection criteria to the charged kaon and K_S candidates, and use exactly the same criteria to select an additional pion and reconstruct the $K^{*0} \to K^+\pi^-$ and $K^{*+} \to K_S\pi^+$ decays. Therefore we set

$$\varepsilon_0 = \varepsilon_c. \quad (23)$$

This relation is confirmed by simulation. We assign a systematic uncertainty related to this relation, as discussed in Sec. VIII. From Eqs. (20)–(23), we obtain

$$f_K = \frac{N(K_S)}{N(K^{*+} \to K_S\pi^+)} f_{K^{*0}}. \quad (24)$$

We use a similar relation to obtain the quantity F_K of $K \to \mu$ tracks in the like-sign dimuon sample:

$$F_K = \frac{N(K_S)}{N(K^{*+} \to K_S\pi^+)} F_{K^{*0}}, \quad (25)$$

where $F_{K^{*0}}$ is the fraction of $K^{*0} \to K^+\pi^-$ decays with $K \to \mu$ in the like-sign dimuon sample. The numbers $N(K_S)$ and $N(K^{*+} \to K_S\pi^+)$ are obtained from the inclusive muon sample.

Since the kaon track parameters must be known to reconstruct the K^{*0} meson, these measurements of f_K and F_K require the kaons to decay after being reconstructed in the central-tracking system. A small number of kaon decays occur close to the interaction point, so that the muon track is reconstructed by the tracker. These muons are counted in the inclusive muon and the like-sign dimuon samples, but do not contribute to the measurement of the $K \to \mu$ fraction, because their parameters differ significantly from the parameters of the original kaon, and they do not produce a narrow K^{*0} meson peak. The fractions F_K and f_K measured in exclusive decays are therefore divided by a factor C that corresponds to the fraction of correctly reconstructed kaons among all $K \to \mu$ tracks. This factor is calculated from simulation as

$$C = 0.938 \pm 0.006. \quad (26)$$

Since the mean decay length of kaons in the laboratory frame is much longer than the size of the D0 detector, the value of C is determined mainly by the detector geometry, and its value is similar for both $K \to \mu$ and $\pi \to \mu$ tracks. Therefore, we use the same coefficient C for the computation of the fraction of $\pi \to \mu$ described in Sec. VII. The difference in this coefficient for kaon and pion tracks observed in simulation is taken as the uncertainty on its value. The uncertainties from the event generation and reconstruction produce a smaller impact on this coefficient.

Details of $K_S \to \pi^+\pi^-$, $K^{*0} \to K^+\pi^-$, and $K^{*+} \to K_S\pi^+$ selections and the fitting procedure to measure the number of these decays are given in Appendix B. All quantities in Eqs. (24) and (25) are obtained as a function of the measured transverse momentum of the kaon. The measured number of $K^{*0} \to K^+\pi^-$ decays with $K \to \mu$ in a given p_T range is normalized by the total number of muons in that interval. The fraction $F_{K^{*0}}$ includes a multiplicative factor of 2, because there are two muons in a like-sign dimuon event, and by definition it is normalized to the number of like-sign dimuon events. Figure 2 and Table III give the resulting fractions f_K and F_K for different p_T bins. Only statistical uncertainties are given; systematic uncertainties are discussed in Sec. VIII. The difference in the absolute value and in the p_T dependence of f_K and F_K may be due to a different composition of the inclusive muon and like-sign dimuon samples, and due to the statistical fluctuations. In addition to the fitting procedure discussed in Appendix B, the ratio F_K/f_K is also measured by an alternative null fit method presented in Appendix E. The agreement between the two methods is very good; therefore we exclude the fitting procedure as the source of difference between f_K and F_K.

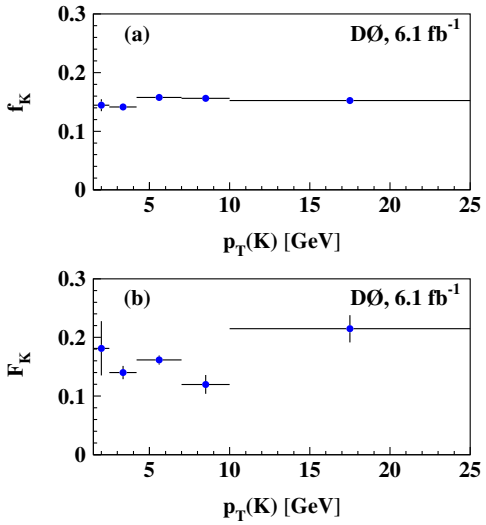

FIG. 2 (color online). The fraction of $K \to \mu$ tracks in the inclusive muon sample (a) and the like-sign dimuon sample (b), both as a function of the p_T of the kaon.

TABLE III. Fractions f_K and F_K for different muon p_T bins. The correspondence between the bin number and the p_T range is given in Table I. The last line shows the weighted average of these quantities obtained with weights given by the fraction of muons in a given p_T interval f_μ^i (F_μ^i) in the inclusive muon (dimuon) sample. Only the statistical uncertainties are given.

Bin	$f_K \times 10^2$	$F_K \times 10^2$
0	14.45 ± 1.02	18.13 ± 4.62
1	14.14 ± 0.26	14.00 ± 1.14
2	15.78 ± 0.20	16.14 ± 0.77
3	15.63 ± 0.35	11.97 ± 1.60
4	15.26 ± 0.56	21.47 ± 2.31
All	15.46 ± 0.14	15.38 ± 0.57

VI. MEASUREMENT OF $P(\pi \to \mu)/P(K \to \mu)$ AND $P(p \to \mu)/P(K \to \mu)$

The probability $P(K \to \mu)$ for a kaon to be misidentified as a muon is measured using $\phi \to K^+K^-$ decays. Similarly, we use $K_S \to \pi^+\pi^-$ and $\Lambda \to p\pi^-$ decays [13] to measure the probabilities $P(\pi \to \mu)$ and $P(p \to \mu)$, respectively. In all cases we measure the number N_μ of decays in which the candidate particle satisfies the muon selection criteria defined in Sec. III, and the number of decays $N_{\rm tr}$ in which the tested particle satisfies the track selection criteria. When both kaons (pions) from $\phi \to K^+K^-$ ($K_S \to \pi^+\pi^-$) satisfy the selection criteria, they contribute twice. The details of the event selections and of the fitting procedure used to extract the number of ϕ, K_S, and Λ decays are given in Appendix B. The ratio of $N_\mu(\phi)$ to $N_{\rm tr}(\phi)$ defines $P(K \to \mu)\varepsilon(\mu)$, where $\varepsilon(\mu)$ is the efficiency of muon identification. In the same way, the ratio of $N_\mu(K_S)$ to $N_{\rm tr}(K_S)$ yields $P(\pi \to \mu)\varepsilon(\mu)$, and the ratio of $N_\mu(\Lambda)$ to $N_{\rm tr}(\Lambda)$ gives the quantity $P(p \to \mu)\varepsilon(\mu)$. The ratios $P(\pi \to \mu)/P(K \to \mu)$ and $P(p \to \mu)/P(K \to \mu)$ are obtained from

$$\frac{P(\pi \to \mu)}{P(K \to \mu)} = \frac{N_\mu(K_S)/N_{\rm tr}(K_S)}{N_\mu(\phi)/N_{\rm tr}(\phi)}, \qquad \frac{P(p \to \mu)}{P(K \to \mu)} = \frac{N_\mu(\Lambda)/N_{\rm tr}(\Lambda)}{N_\mu(\phi)/N_{\rm tr}(\phi)}. \tag{27}$$

Since the initial selection for this measurement requires at least one identified muon, we determine all these quantities in the subsample of single muon triggers that contain at least one muon not associated with the $K \to \mu$, $\pi \to \mu$, or $p \to \mu$ transitions.

We measure all these parameters as a function of the original particle's transverse momentum. Figures 3 and 4 show the ratios $P(\pi \to \mu)/P(K \to \mu)$ and $P(p \to \mu)/P(K \to \mu)$, respectively, with the mean values averaged over p_T determined to be

$$P(\pi \to \mu)/P(K \to \mu) = 0.540 \pm 0.029, \tag{28}$$

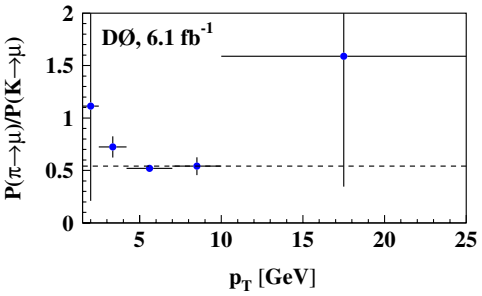

FIG. 3 (color online). The ratio $P(\pi \to \mu)/P(K \to \mu)$ as a function of the hadron transverse momentum. The horizontal dashed line shows the mean value of this ratio.

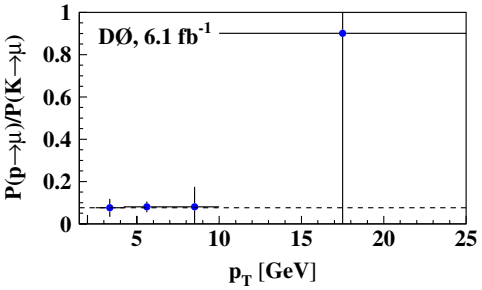

FIG. 4 (color online). The ratio $P(p \to \mu)/P(K \to \mu)$ as a function of the particle transverse momentum. The horizontal dashed line shows the mean value of this ratio.

$$P(p \to \mu)/P(K \to \mu) = 0.076 \pm 0.021. \tag{29}$$

The dominant uncertainty in Eqs. (28) and (29) stems from the limited statistics of data, and the contribution of all other uncertainties is much smaller. The probability of a pion to be misidentified as a muon is much larger than that of a proton because the dominant contribution to this probability comes from the $\pi^- \to \mu^-\bar{\nu}$ decay. The measured ratios (28) and (29) agree well with the results obtained from MC simulation, where we obtain $P(\pi \to \mu)/P(K \to \mu)(\text{MC}) = 0.530 \pm 0.011$ and $P(p \to \mu)/P(K \to \mu)(\text{MC}) = 0.050 \pm 0.003$.

VII. MEASUREMENT OF f_π, f_p, F_π, F_p

The fraction f_π of $\pi \to \mu$ tracks in the inclusive muon sample can be expressed as

$$f_\pi = f_K \frac{P(\pi \to \mu)}{P(K \to \mu)} \frac{n_\pi}{n_K}, \tag{30}$$

where the measurement of the fraction f_K is described in Sec. V, that of the ratio $P(\pi \to \mu)/P(K \to \mu)$ in Sec. VI, and the quantities n_π and n_K are the mean multiplicities of pions and kaons in $p\bar{p}$ interactions. In a similar way, the fraction f_p of $p \to \mu$ tracks is determined from

$$f_p = f_K \frac{P(p \to \mu)}{P(K \to \mu)} \frac{n_p + n_f}{n_K}, \tag{31}$$

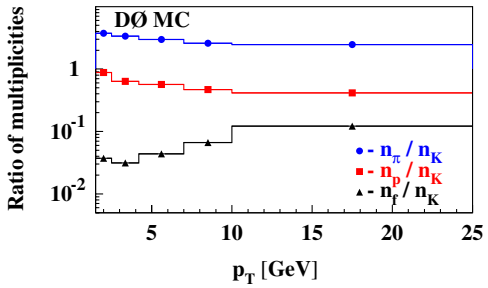

FIG. 5 (color online). The ratio of multiplicities n_π/n_K, n_p/n_K, and n_f/n_K as a function of the transverse momentum obtained from PYTHIA.

where n_p is the average number of protons produced in $p\bar{p}$ interactions. We include in the fraction f_p the contribution from the number n_f of false tracks, reconstructed from random combinations of hits. The impact of false tracks on the final result is found to be small and is taken into account in the systematic uncertainty.

The values of n_K, n_π, n_p, and n_f are taken from the PYTHIA simulation of inclusive hadronic interactions. We count the number of particles satisfying the track selection criteria in the simulated interactions, and obtain the dependence of the ratios n_π/n_K, n_p/n_K, and n_f/n_K on the particle p_T shown in Fig. 5.

Both f_π and f_p are measured as a function of the particle p_T. However, they are poorly defined in the first and last bins due to low statistics. Therefore, we combine these quantities for bins 0 and 1 and for bins 3 and 4.

Figure 6 and Table IV provide the measured fractions f_π and f_p for different p_T bins. Only statistical uncertainties are given. The systematic uncertainties related to these quantities are discussed in Sec. VIII.

TABLE IV. Fractions f_π, f_p, F_π, and F_p for different p_T bins. The correspondence between the bin number and the momentum range is given in Table I. The last line shows the weighted averages obtained with weights given by the fraction of muons in a given p_T interval f_μ^i in the inclusive muon sample. Only the statistical uncertainties are given.

Bin	$f_\pi \times 10^2$	$f_p \times 10^2$	$F_\pi \times 10^2$	$F_p \times 10^2$
0–1	35.6 ± 4.9	0.6 ± 0.4	32.2 ± 5.1	0.5 ± 0.4
2	24.3 ± 1.6	0.7 ± 0.2	22.4 ± 1.8	0.7 ± 0.2
3–4	21.7 ± 3.4	0.7 ± 0.7	19.0 ± 3.4	0.6 ± 0.6
All	25.8 ± 1.4	0.7 ± 0.2	24.9 ± 1.5	0.6 ± 0.2

The fractions F_π and F_p in the like-sign dimuon sample are determined in a similar way:

$$F_\pi = F_K \frac{P(\pi \to \mu)}{P(K \to \mu)} \frac{N_\pi}{N_K},$$
$$F_p = F_K \frac{P(p \to \mu)}{P(K \to \mu)} \frac{N_p + N_f}{N_K}, \tag{32}$$

where the quantities N_K, N_π, N_p, and N_f represent the average numbers of kaons, pions, protons, and false tracks for events with two identified muons with the same charge. The simulation shows that the ratio N_π/N_K can be approximated as

$$\frac{N_\pi}{N_K} = (0.90 \pm 0.05)\frac{n_\pi}{n_K}. \tag{33}$$

The main uncertainty in this value is due to the simulation of pion and kaon multiplicities in $p\bar{p}$ interactions and is discussed in Sec. VIII. The ratio N_p/N_K is also consistent with the factor given in Eq. (33). The value of N_π/N_K is

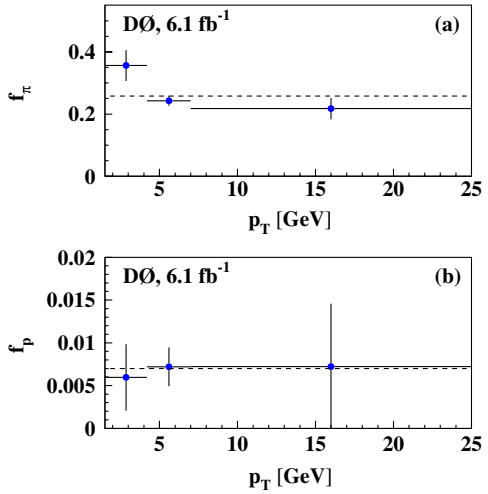

FIG. 6 (color online). The fraction of (a) $\pi \to \mu$ tracks and (b) $p \to \mu$ tracks in the inclusive muon sample as a function of the track transverse momentum. The horizontal dashed lines show the mean values of these fractions.

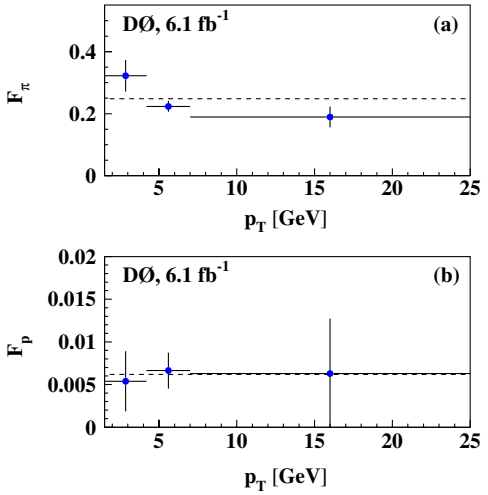

FIG. 7 (color online). The fraction of (a) $\pi \to \mu$ tracks and (b) $p \to \mu$ tracks in the like-sign dimuon sample as a function of the track transverse momentum. The horizontal dashed lines show the mean values of these fractions.

smaller than that of n_π/n_K because the main contribution in the sample with one identified muon comes from semileptonic decays of b and c quarks, which usually also contain at least one kaon. Since the number of simulated events with one identified muon is small, we obtain the ratios N_π/N_K and $(N_p + N_f)/N_K$ using the approximation of Eq. (33), i.e., multiplying the quantities n_π/n_K and $(n_p + n_f)/n_K$ by the factor 0.90 ± 0.05. Figure 7 and Table IV give the fractions F_π and F_p for different p_T bins. Only the statistical uncertainties of the simulation are given. The systematic uncertainties related to these quantities are discussed in Sec. VIII. As in the case of f_π and f_p, the mean value of these quantities are used in bins 0 and 1 and for bins 3 and 4.

VIII. SYSTEMATIC UNCERTAINTIES OF BACKGROUND FRACTIONS

We use Eqs. (22) and (23) to derive the fractions f_K and F_K, and verify the validity of Eq. (23) in simulation, and find that

$$(\varepsilon_c/\varepsilon_0)_{\mathrm{MC}} = 0.986 \pm 0.029, \tag{34}$$

where the uncertainty reflects only the statistics of the Monte Carlo simulation. The ratio $R(K^{*+})/R(K^{*0})$ measured in simulation is

$$R(K^{*+})/R(K^{*0}) = 0.959 \pm 0.035. \tag{35}$$

The validity of Eq. (22) in simulation relies mainly on the assumptions used in the fragmentation and hadronization processes in the event generator. To confirm the validity of Eq. (22), we use the existing experimental data on K^+, K_S, K^{*0}, and K^{*+} multiplicities in jets, which were obtained at e^+e^- colliders at different center-of-mass energies [2]. From these data we obtain

$$R(K^{*+})/R(K^{*0}) = 1.039 \pm 0.075. \tag{36}$$

The simulation and data are consistent, and we assign a relative uncertainty of 7.5% to both f_K and F_K from the assumption of Eq. (22). We also assign an uncertainty of 4% due to the fitting procedure used to extract the numbers of K^{*+} and K^{*0} events. This uncertainty is obtained by varying the background parametrization and the fitting range. Since the same background model is used to obtain the number of K^{*0} events, both in the inclusive muon and the like-sign dimuon samples, this uncertainty is taken to be the same for f_K and F_K. Adding all contributions in quadrature, and including the uncertainty in Eq. (26), we find a relative systematic uncertainty of 9.0% in f_K and F_K, with a 100% correlation between the two.

We assign an additional uncertainty of 2.0% on F_K due to the description of the background in the inclusive muon and like-sign dimuon events. This uncertainty is estimated by varying the background parametrization and range used for fitting, and by comparing with the results of the alternative fitting method presented in Appendix E.

We use the ratio $N(K_S)/N(K^{*+} \to K_S\pi^+)$ to measure both f_K and F_K, which is equivalent to the statement that the ratios $F_{K^{*0}}/F_K$ and $f_{K^{*0}}/f_K$ are identical, i.e., that the fraction of kaons originating from K^{*0} is the same in the inclusive muon and in the like-sign dimuon samples. This is validated in simulation with an uncertainty of 3% limited by the statistics of the simulation, which we assign as an additional systematic uncertainty to the fraction F_K. We also performed a measurement of the F_{K_S}/f_{K_S} ratio, where f_{K_S}, F_{K_S} are the fractions of $K_S \to \pi^+\pi^-$ decays with one pion misidentified as a muon in the inclusive muon and the like-sign dimuon samples, respectively. The ratios F_{K_S}/f_{K_S} and F_K/f_K are expected to be the same due to isospin invariance, and we find that they agree within the statistical and systematic uncertainties.

The uncertainties on the background fractions f_π, F_π, f_p, and F_p have an additional contribution from the ratios of multiplicities n_π/n_K and n_p/n_K extracted from the simulation. To test the validity of the simulation, we measure the multiplicity of kaons in the inclusive muon sample. We select events with one reconstructed muon and at least one additional charged particle that satisfies the track selection criteria. We determine the fraction of kaons among these tracks using the same method as in Sec. V, i.e., we find the fraction of tracks from the $K^{*0} \to K^+\pi^-$ decay and convert this into the fraction of kaons. We compare the kaon multiplicity in data using this method with that measured in the simulation, and we find that they agree within 10%. Since part of this difference can be attributed to the uncertainties from the assumptions of Eqs. (22) and (23), and part is due to the fitting procedure described above, we find that the uncertainty of the kaon multiplicity in the simulation does not exceed 4%, and we assign this uncertainty to both quantities n_π/n_K and n_p/n_K. We also assign this 4% uncertainty to the Eq. (33) used to derive the values of N_π/N_K and N_p/N_K.

Any falsely reconstructed track identified as a muon is treated in the analysis in the same way as a proton. We check the impact of this approach by completely removing the contribution of false tracks, or by increasing their contribution by a factor of 10, and the final value of A^b_{sl} changes by less than 0.000 16. We include this difference as the systematic uncertainty on the contribution from false tracks.

IX. MEASUREMENT OF f_S, F_{SS}

We use the measurements of the fractions of background muons in the long category, obtained in the previous sections to evaluate the fraction of muons in the short category. In the inclusive muon sample the fraction f_S is determined as

$$f_S = 1 - f_K - f_\pi - f_p. \tag{37}$$

We check through simulation that the contribution from all other sources to the inclusive muon sample, such as $K_L \to \pi\mu\nu$ decays or the semileptonic decays of hyperons, is negligible. The muons from $\tau \to \mu\bar{\nu}_\mu\nu_\tau$ are included by definition in the f_S. The fraction f_S is measured separately in each muon p_T bin and then a weighted average is calculated with weights given by the fraction of muons in a given p_T interval f_μ^i in the inclusive muon samples. From data, we obtain

$$f_S = 0.581 \pm 0.014 \text{ (stat)} \pm 0.039 \text{ (syst)}, \quad (38)$$

where the systematic uncertainty comes from the uncertainty on the background fractions described in Sec. VIII.

To check the procedure for determining the background fractions, the composition of the inclusive muon sample in data is compared to that from simulation in Table V, where only statistical uncertainties for both data and simulation are shown. The agreement between data and simulation is very good, and the remaining differences are within the assigned systematic uncertainties. Although the values given in Table V for data and for simulation are not independent, some, such as f_K and $P(\pi \to \mu)/P(K \to \mu)$ used to derive f_π, are measured directly in data. As a consequence, this result can be used as an additional confirmation of the validity of our method.

The background fractions F_K, F_π, and F_p are obtained from the same weighted average used for Eq. (38) of the quantities measured in each p_T interval i, starting from the values given in Secs. V and VII (F_μ^i is used as weight instead of f_μ^i). Using Eq. (15), we obtain

$$F_{\text{bkg}} = 0.409 \pm 0.019 \text{ (stat)} \pm 0.040 \text{ (syst)}. \quad (39)$$

To evaluate the fraction F_{SS} in the like-sign dimuon sample, we take into account that, in some events, both muons belong to the L category. The fraction of these events in all events with at least one L muon is measured in simulation and found to be

$$\frac{F_{LL}}{F_{SL} + F_{LL}} = 0.220 \pm 0.012. \quad (40)$$

The uncertainty in Eq. (40) includes the 4% systematic uncertainty related to the multiplicity of different particles in the simulation, as discussed in Sec. VIII. Using Eqs. (15), (39), and (40), we obtain

$$F_{LL} = 0.074 \pm 0.003 \text{ (stat)} \pm 0.008 \text{ (syst)}, \quad (41)$$

TABLE V. Fractions f_S, f_K, f_π, and $f_p + f_f$, measured in data and in simulation (MC). Only the statistical uncertainties on these measurements are shown.

	$f_S \times 10^2$	$f_K \times 10^2$	$f_\pi \times 10^2$	$(f_p + f_f) \times 10^2$
Data	58.1 ± 1.4	15.5 ± 0.2	25.9 ± 1.4	0.7 ± 0.2
MC	59.0 ± 0.3	14.5 ± 0.2	25.7 ± 0.3	0.8 ± 0.1

and, finally, from Eqs. (16), (39), and (41) we obtain

$$F_{SS} = 0.665 \pm 0.016 \text{ (stat)} \pm 0.033 \text{ (syst)}. \quad (42)$$

X. MEASUREMENT OF δ

Table III of Ref. [17] gives a complete list of the contributions to the dimuon charge asymmetry that are caused by detector effects. The largest of these effects is $\approx 3\%$. The reversal of magnet polarities is a characteristic of the D0 experiment that allows the cancellation at first order of these detector effects, reducing any charge asymmetry introduced by the track reconstruction considerably [17].

Higher-order effects result in a small residual reconstruction asymmetry at the 10^{-3} level. This asymmetry is measured using $J/\psi \to \mu^+\mu^-$ decays. We select events that pass at least one dimuon trigger and have at least one identified muon and one additional particle of opposite charge that satisfies the track selection criteria of Sec. III. We verify in Appendixes C and D that the track reconstruction and trigger selection do not introduce an additional charge asymmetry. The residual asymmetry is measured as a function of the muon transverse momentum. The probability to identify a muon with charge $Q = \pm 1$ and p_T corresponding to bin i is denoted by $P_i(1 + Q\delta_i)$, where P_i is the mean probability for positive and negative muons, and δ_i is the muon detection asymmetry we want to measure. The probability of identifying the second muon with p_T in bin j, provided that the first muon has p_T in bin i, is denoted by $P_j^i(1 + Q\delta_j)$.

The number of events N_{ij} with a positive muon in bin i and negative muon in bin j is

$$N_{ij} = NP_i(1 + \delta_i)P_j^i(1 - \delta_j), \quad (43)$$

where N is the total number of selected $J/\psi \to \mu^+\mu^-$ decays. The number of events with only one selected muon of charge Q is

$$N_{iQ} = NP_i(1 + Q\delta_i)\left(1 - \sum_{j=0}^{4} P_j^i(1 - Q\delta_j)\right), \quad (44)$$

where the sum extends over the five transverse momentum intervals.

The probabilities P_i and P_j^i are not independent. From Eq. (43), we have the following normalization condition:

$$P_iP_j^i = P_jP_i^j. \quad (45)$$

In addition, since the total probability to identify the muon is $P_{\text{tot}} = \sum_{i=0}^{4} P_i$, we get the following normalization condition:

$$(P_{\text{tot}})^2 = \sum_{i,j=0}^{4} P_iP_j^i. \quad (46)$$

Experimentally we measure the quantities N_{ii}, Σ_{ij}, Δ_{ij} $(i < j)$, Σ_i, and Δ_i, which can be expressed as

$$\begin{aligned} N_{ii} &= NP_iP_i^i, \qquad \Sigma_{ij} \equiv N_{ij} + N_{ji} = 2NP_iP_j^i, \\ \Delta_{ij} &\equiv N_{ij} - N_{ji} = 2NP_iP_j^i(\delta_i - \delta_j), \\ \Sigma_i &\equiv N_{i+} + N_{i-} = 2NP_i(1 - P_{\rm sum}^i), \\ \Delta_i &\equiv N_{i+} - N_{i-} = 2NP_i(1 - P_{\rm sum}^i)(\delta_i + \delta_{\rm sum}^i), \end{aligned} \tag{47}$$

where

$$P_{\rm sum}^i = \sum_{j=0}^{4} P_j^i$$

and

$$\delta_{\rm sum}^i = \left(\sum_{j=0}^{4} P_j^i \delta_j\right)/(1 - P_{\rm sum}^i).$$

Since the number of measured quantities is greater than the number of unknowns, P_i, P_j^i, and δ_i can be obtained from Eqs. (45)–(47) by minimizing the χ^2 of the difference between the observed and expected quantities. The quantities N_{ii}, Σ_{ij}, Δ_{ij} $(i < j)$, Σ_i, and Δ_i are obtained from fits to the J/ψ mass peak in the dimuon invariant mass distribution $M(\mu^+\mu^-)$ in each of the five p_T bins. The J/ψ signal is described by the sum of two Gaussians. An additional Gaussian is included to take into account the contribution from the ψ'. The background is parametrized by a third degree polynomial. The mean position and rms of all Gaussian functions in the fit of Δ_{ij} and Δ_i are fixed to the values obtained in the fit of the corresponding quantities Σ_{ij} and Σ_i. Examples of the fits are shown in Figs. 8 and 9. The values of δ_i obtained as a function of the muon p_T are given in Table VI and are shown in Fig. 10. The correlations between values of δ_i in different bins are given in Table VII. The weighted average for the residual muon asymmetry in the inclusive muon and the like-sign dimuon samples, calculated using weights given by the fraction of muons in a given p_T interval f_μ^i (F_μ^i) in the inclusive muon (dimuon) sample, are given, respectively, by

$$\delta = \sum_{i=0}^{4} f_\mu^i \delta_i = -0.000\,76 \pm 0.000\,28, \tag{48}$$

$$\Delta = \sum_{i=0}^{4} F_\mu^i \delta_i = -0.000\,68 \pm 0.000\,23, \tag{49}$$

where only the statistical uncertainties are given. The correlations among different δ_i are taken into account. These small values of the residual muon reconstruction asymmetry are a direct consequence of the regular reversal of the magnets polarities in the D0 experiment.

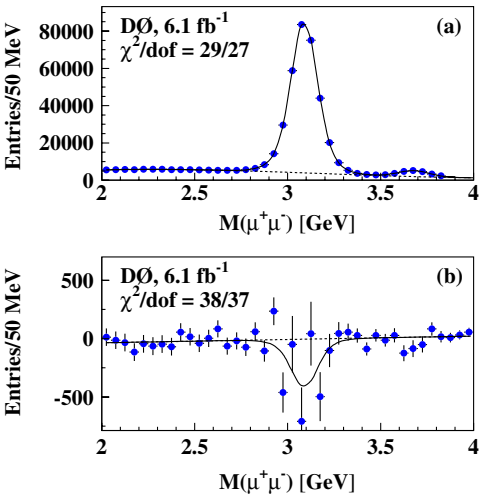

FIG. 8 (color online). The $\mu^+\mu^-$ invariant mass distributions used to obtain (a) $\Sigma_{23} = N_{23} + N_{32}$ and (b) $\Delta_{23} = N_{23} - N_{32}$. The solid lines present the result of the fit; the dashed lines show the nonresonant background contribution.

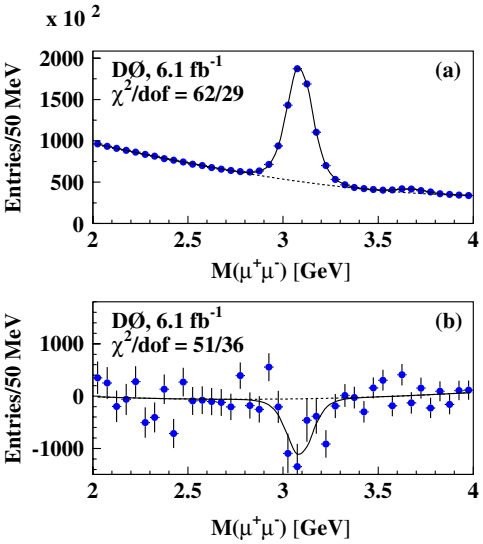

FIG. 9 (color online). The $\mu^+\mu^-$ invariant mass distributions used to obtain (a) $\Sigma_2 = N_{2+} + N_{2-}$ and (b) $\Delta_2 = N_{2+} - N_{2-}$. The solid lines present the result of the fit; the dashed lines show the nonresonant background contribution.

TABLE VI. Muon reconstruction asymmetry δ_i for different muon p_T bins. The correspondence between the bin number and the p_T range is given in Table I. Only the statistical uncertainties are given.

Bin	δ_i
0	$-0.002\,03 \pm 0.001\,94$
1	$-0.000\,45 \pm 0.000\,59$
2	$-0.001\,30 \pm 0.000\,48$
3	$+0.000\,75 \pm 0.001\,25$
4	$+0.001\,62 \pm 0.002\,30$

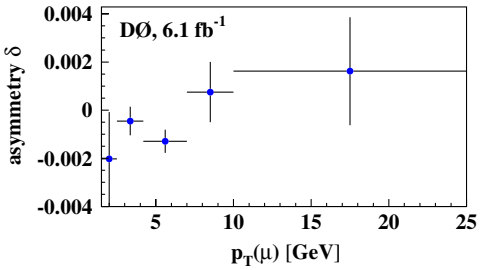

FIG. 10 (color online). Muon reconstruction asymmetry as a function of the muon p_T.

TABLE VII. Correlation coefficients among values of δ_i in different bins. The correspondence between the bin number and the p_T range is given in Table I.

Bin	0	1	2	3	4
0	+1.000	−0.189	−0.155	+0.024	−0.051
1	−0.189	+1.000	−0.449	−0.117	−0.059
2	−0.155	−0.449	+1.000	−0.242	−0.124
3	+0.024	−0.117	−0.242	+1.000	−0.006
4	−0.051	−0.059	−0.124	−0.006	+1.000

XI. MEASUREMENT OF a_K, a_π, a_p

The largest detector-related charge asymmetry is produced by $K \to \mu$ tracks. It is caused, as discussed in Sec. II, by the difference between the K^-N and K^+N interaction cross sections [2], resulting in a positive charge asymmetry of muons coming from kaon decay or punchthrough.

The asymmetry a_K of $K \to \mu$ tracks is measured directly in data using $K^{*0} \to K^+\pi^-$ and $\phi \to K^+K^-$ decays. In both cases we select candidates with $K \to \mu$ tracks, in the entire inclusive muon sample. We calculate separate mass distributions for positive and negative $K \to \mu$ tracks, and fit the sum and the difference of these distributions to extract the quantity Δ_K, corresponding to the difference in the number of K^{*0} or ϕ meson decays with positive and negative $K \to \mu$ tracks, and the quantity Σ_K, corresponding to their sum. The selection of events and the fitting procedure used to extract the number of signal decays are described in Appendix B. The asymmetry a_K is measured as

$$a_K = C\Delta_K/\Sigma_K, \tag{50}$$

where the coefficient C is the fraction of correctly reconstructed kaons among all $K \to \mu$ tracks as in Eq. (26). In this measurement of a_K, we require that the kaon decays after having been reconstructed in the tracking system, since its track parameters must be measured in order to reconstruct the K^{*0} or ϕ meson. However, the $K \to \mu$ tracks in the inclusive sample also include kaons decaying before being reconstructed in the tracker. Since the kaon asymmetry is caused by the interactions of kaons with the material of the detector, and the amount of material near the interaction point is negligible, the kaons decaying before being reconstructed by the tracker do not produce any significant asymmetry. They contribute only in the denominator of Eq. (50). The factor C takes into account the contribution of these tracks. Its numerical value is given in Eq. (26). It should be noted that this factor cancels in the products $f_K a_K$, etc., since both f_K and a_K are measured using the correctly reconstructed $K \to \mu$ tracks.

Figure 11(a) shows the value of $a_K(K^{*0})$ measured in $K^{*0} \to K^+\pi^-$ decay as a function of the p_T of the $K \to \mu$ track. The asymmetry in $\phi \to K^+K^-$ decays $a_K^{\rm meas}$ has to be corrected for the charge asymmetry of the second kaon track $a_K^{\rm track}$:

$$a_K(\phi) = a_K^{\rm meas} - a_K^{\rm track}. \tag{51}$$

The kaon track reconstruction asymmetry $a_K^{\rm track}$ is discussed and measured as a function of kaon momentum in [23] using the decay $D^{*+} \to D^0\pi^+$ with $D^0 \to K^-\mu^+\nu$, and is taken from that article. It is convolved with the p_T distribution of the second kaon for each bin of the $K \to \mu$ p_T. Figure 11(b) shows the resulting asymmetry $a_K(\phi)$.

The two measurements of a_K are consistent. The χ^2/d.o.f. for their difference is 5.40/5. Therefore they can be combined and the resulting asymmetry a_K is shown in Fig. 12 and in Table VIII. Because of the requirement of $p_T > 4.2$ GeV or $|p_z| > 6.3$ GeV, the first two bins in Fig. 12 correspond to muons that traverse the forward toroids of the D0 detector. These muons have a larger momentum and a longer path length before the calorimeter than central muons. As a result, a_K drops at low p_T.

The asymmetry a_π of $\pi \to \mu$ tracks and the asymmetry a_p of $p \to \mu$ tracks are expected to be much smaller. We measure these asymmetries using $K_S \to \pi^+\pi^-$ and $\Lambda \to p\pi^-$ decays, respectively. The details of the K_S and Λ

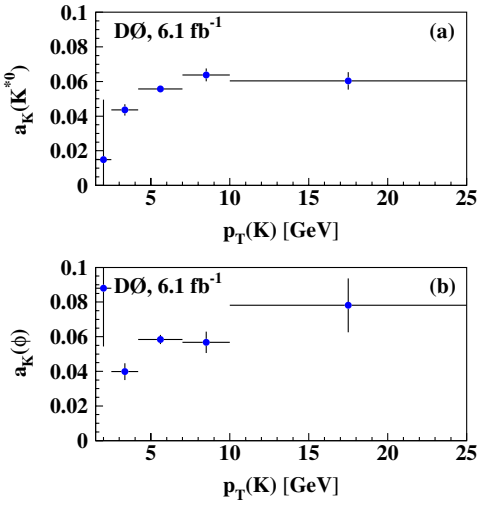

FIG. 11 (color online). The asymmetry a_K measured with (a) $K^{*0} \to K^+\pi^-$ and (b) $\phi \to K^+K^-$ decays as a function of the $K \to \mu$ p_T.

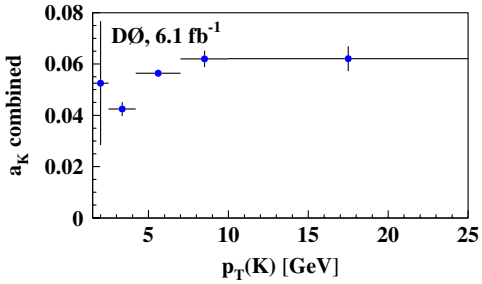

FIG. 12 (color online). The combined asymmetry a_K as a function of p_T.

selections are given in Appendix B. The technique used to measure the asymmetry is the same as in a_K measurement. The same factor C is used to measure the asymmetry a_π from $K_s \to \pi^+\pi^-$ decays. The uncertainty in C takes into account its difference for kaon and pion tracks. Since the proton is stable, this factor is not used in the computation of the asymmetry of $p \to \mu$ tracks.

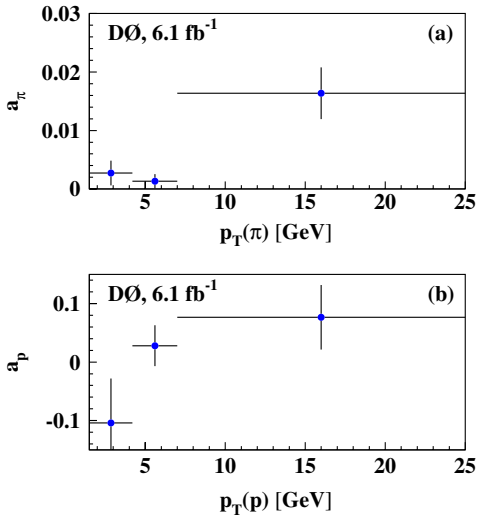

FIG. 13 (color online). The asymmetry (a) a_π and (b) a_p as a function of the p_T of the pion and proton, respectively.

TABLE VIII. Asymmetries a_K, a_π, and a_p for different p_T bins. The correspondence between the bin number and p_T range is given in Table I. The last line shows the mean asymmetries averaged over the inclusive muon sample. Only the statistical uncertainties are given.

Bin	a_K	a_π	a_p
0	$+0.0526 \pm 0.0242$	$+0.0027 \pm 0.0021$	-0.104 ± 0.076
1	$+0.0424 \pm 0.0027$		
2	$+0.0564 \pm 0.0013$	$+0.0013 \pm 0.0012$	$+0.028 \pm 0.035$
3	$+0.0620 \pm 0.0032$	$+0.0164 \pm 0.0044$	$+0.077 \pm 0.055$
4	$+0.0620 \pm 0.0048$		
All	$+0.0551 \pm 0.0011$	$+0.0025 \pm 0.0010$	$+0.023 \pm 0.028$

The asymmetries a_π and a_p are shown in Fig. 13 as a function of the p_T of the $\pi \to \mu$ and $p \to \mu$ tracks, respectively. The values of these asymmetries and their averages are listed in Table VIII for different p_T bins. We use the mean value of these quantities in bins 0 and 1 and in bins 3 and 4 since the statistics available in the first and last bin are not sufficient to perform separate measurements.

The asymmetries A_K, A_π, and A_p are obtained from a_K, a_π, and a_p using Eq. (18) (and analogous relations for pions and protons).

XII. CORRECTIONS DUE TO BACKGROUND ASYMMETRIES

The corrections for the asymmetries of the background, obtained from Tables I, III, IV, and VIII, are summarized in Tables IX and X. The values $f_K a_K$, $F_K A_K$, etc., are computed by averaging the corresponding quantities with weights given by the fraction of muons in a given p_T interval f_μ^i (F_μ^i) in the inclusive muon (dimuon) sample; see Eqs. (17) and (18). We use the mean value of f_π, F_π, f_p, F_p, a_π, and a_p in bins 0 and 1 and in bins 3 and 4 as the statistics available in the first and last bin are not sufficient to perform separate measurements.

TABLE IX. Corrections due to background asymmetries $f_K a_K$, $f_\pi a_\pi$, and $f_p a_p$ for different p_T bins. The last line shows the weighted averages obtained using weights given by the fraction of muons in a given p_T interval f_μ^i in the inclusive muon sample. Only the statistical uncertainties are given.

Bin	$f_K a_K \times 10^2$	$f_\pi a_\pi \times 10^2$	$f_p a_p \times 10^2$
0	$+0.760 \pm 0.353$	$+0.095 \pm 0.076$	-0.061 ± 0.060
1	$+0.600 \pm 0.040$		
2	$+0.889 \pm 0.023$	$+0.033 \pm 0.030$	$+0.020 \pm 0.026$
3	$+0.968 \pm 0.054$	$+0.337 \pm 0.109$	$+0.053 \pm 0.067$
4	$+0.946 \pm 0.081$		
All	$+0.854 \pm 0.018$	$+0.095 \pm 0.027$	$+0.012 \pm 0.022$

TABLE X. Corrections due to background asymmetries $F_K A_K$, $F_\pi A_\pi$, and $F_p A_p$ for different p_T bins. The last line shows the weighted averages obtained using weights given by the fraction of muons in a given p_T interval F_μ^i in the dimuon sample. Only the statistical uncertainties are given.

Bin	$F_K A_K \times 10^2$	$F_\pi A_\pi \times 10^2$	$F_p A_p \times 10^2$
0	$+0.953 \pm 0.501$	$+0.086 \pm 0.069$	-0.056 ± 0.054
1	$+0.594 \pm 0.061$		
2	$+0.910 \pm 0.048$	$+0.030 \pm 0.027$	$+0.019 \pm 0.024$
3	$+0.741 \pm 0.106$	$+0.294 \pm 0.098$	$+0.046 \pm 0.058$
4	$+1.332 \pm 0.176$		
All	$+0.828 \pm 0.035$	$+0.095 \pm 0.025$	$+0.000 \pm 0.021$

XIII. ASYMMETRIES a_S AND A_S

In the absence of new particles or interactions, the only noninstrumental source of the asymmetries a_S and A_S is the semileptonic charge asymmetry $A^b_{\rm sl}$ given by Eq. (5). Both a_S and A_S are proportional to $A^b_{\rm sl}$, through the coefficients

$$c_b \equiv a_S/A^b_{\rm sl}, \tag{52}$$

$$C_b \equiv A_S/A^b_{\rm sl}, \tag{53}$$

which are determined from simulation.

The decays producing an S muon in the inclusive muon sample, and their weights relative to the semileptonic decay $b \to \mu X$ [13], are listed in Table XI. All weights are computed using simulated events. The main process, denoted as T_1, is the direct semileptonic decay of a b quark. It includes the decays $b \to \mu X$ and $b \to \tau X$, with $\tau \to \mu X$. The weights w_{1a} and w_{1b} for semileptonic decays of B mesons with and without oscillations are computed using the mean mixing probability

$$\chi_0 = f'_d \chi_{d0} + f'_s \chi_{s0}, \tag{54}$$

where f'_d and f'_s are the fractions of B^0_d and B^0_s mesons in a sample of semileptonic B-meson decays, and χ_{d0} and χ_{s0} are the B^0_d and B^0_s mixing probabilities integrated over time. We use the value $\chi_0 = 0.147 \pm 0.011$ measured at the Tevatron and given in [2,24]. The second process T_2 concerns the sequential decay $b \to c \to \mu X$. For simplicity we use the same value of χ_0 to compute the weights w_{2a} and w_{2b} of nonoscillating and oscillating sequential decays $b \to c \to \mu X$. The process T_3 is the decay of a b hadron to a $c\bar{c}$ pair, with either the c or $\bar{c}$ quark producing a muon, while T_4 includes the decays of short-lived mesons η, ω, ρ^0, $\phi(1020)$, J/ψ, and ψ' to a $\mu^+\mu^-$ pair. We take into account both the decays of b hadrons to these particles and their prompt production. The process T_5 represents four-quark production of $b\bar{b}c\bar{c}$ with either the c or $\bar{c}$ quark decaying to a muon. The decays of b or $\bar{b}$ quark to a muon in this process and the four-quark production of $b\bar{b}b\bar{b}$ are taken into account through processes T_1, T_2, and T_3. Finally, the process T_6 involves $c\bar{c}$ production followed by $c \to \mu X$ decay. We separate the processes T_5 and T_6 because only T_5 contributes to the like-sign dimuon sample, while both T_5 and T_6 contribute to the inclusive muon sample.

TABLE XI. Heavy quark decays contributing to the inclusive muon and like-sign dimuon samples. Abbreviations "nos" stand for "nonoscillating" and "osc" for "oscillating." All weights are computed using the MC simulation.

	Process	Weight
T_1	$b \to \mu^- X$	$w_1 \equiv 1$
T_{1a}	$b \to \mu^- X$ (nos)	$w_{1a} = (1 - \chi_0)w_1$
T_{1b}	$\bar{b} \to b \to \mu^- X$ (osc)	$w_{1b} = \chi_0 w_1$
T_2	$b \to c \to \mu^+ X$	$w_2 = 0.113 \pm 0.010$
T_{2a}	$b \to c \to \mu^+ X$ (nos)	$w_{2a} = (1 - \chi_0)w_2$
T_{2b}	$\bar{b} \to b \to c \to \mu^+ X$ (osc)	$w_{2b} = \chi_0 w_2$
T_3	$b \to c\bar{c}q$ with $c \to \mu^+ X$ or $\bar{c} \to \mu^- X$	$w_3 = 0.062 \pm 0.006$
T_4	η, ω, ρ^0, $\phi(1020)$, J/ψ, $\psi' \to \mu^+\mu^-$	$w_4 = 0.021 \pm 0.001$
T_5	$b\bar{b}c\bar{c}$ with $c \to \mu^+ X$ or $\bar{c} \to \mu^- X$	$w_5 = 0.013 \pm 0.002$
T_6	$c\bar{c}$ with $c \to \mu^+ X$ or $\bar{c} \to \mu^- X$	$w_6 = 0.660 \pm 0.077$

The uncertainty in the weights of different processes contains contributions from the uncertainty in the momentum of the generated b hadrons and from the uncertainties of branching fractions for b-hadron decays. We reweight the simulated b-hadron momentum to get agreement of the muon momentum spectrum in data and in MC, and the difference in weights is assigned as the systematic uncertainty on the momentum distribution. The uncertainties in the inclusive branching fractions $B \to \mu X$, $B \to cX$, and $B \to \bar{c}X$ taken from [2] are propagated into the uncertainties on the corresponding weights. We assign an additional uncertainty of 10% to the weights w_5 and w_6 due to the uncertainties on the production cross sections of $c\bar{c}$ and $b\bar{b}c\bar{c}$ processes.

Among all processes listed in Table XI, the process T_{1b} is directly related to the semileptonic charge asymmetry $A^b_{\rm sl}$ (see Appendix A for details). The process T_{2b} produces the flavor-specific charge asymmetry A_{fs}. We set $A_{fs} = -A^b_{\rm sl}$, where the negative sign appears because the charge of the muon in the process T_{2b} is opposite to the charge of the muon in the process T_{1b}. No other process contributes to the charge asymmetry and therefore they just dilute the value of $A^b_{\rm sl}$. The coefficient c_b is found from

$$c_b = \frac{w_{1b} - w_{2b}}{w_1 + w_2 + w_3 + w_4 + w_5 + w_6} = 0.070 \pm 0.006. \tag{55}$$

The computation of the coefficient C_b is more complicated. One of the selections for the like-sign dimuon sample requires that the invariant mass of the two muons be greater than 2.8 GeV. This requirement suppresses the contribution from processes in which both muons arise from the decay of the same quark. The probability that the initial b quark produces a μ^- is

$$P_b \propto w_{1a} + w_{2b} + 0.5(w_3 + w_4 + w_5), \tag{56}$$

where we apply the coefficient 0.5 because processes T_3, T_4, and T_5 produce an equal number of positive and negative muons. The probability that the accompanying $\bar{b}$ quark also produces a μ^- is

$$P_{\bar{b}} \propto w_{1b} + w_{2a} + 0.5(w_3 + w_4 + w_5). \tag{57}$$

The total probability of observing like-sign dimuon events from decays of heavy quarks is

$$P_{\rm tot} \propto P_b P_{\bar{b}}. \tag{58}$$

The probability of processes contributing to the charge

asymmetry of dimuon events is

$$P_{\rm as} \propto w_{1b}[w_{1a} + 0.5(w_3 + w_4 + w_5)] - w_{2b}[w_{2a} + 0.5(w_3 + w_4 + w_5)]. \quad (59)$$

The coefficient C_b is obtained from the ratio

$$C_b = P_{\rm as}/P_{\rm tot} = 0.486 \pm 0.032. \quad (60)$$

This relation assumes that the processes producing the two muons are independent and is verified by calculating the coefficient C_b in simulated like-sign dimuon events. We exclude the process T_6 with $c\bar{c}$ pair production, since the mixing probability of the D^0 meson is small and these events do not contribute significantly to the like-sign dimuon sample. We count the number of direct-direct b-quark decays, $N_{\rm dd}$, of direct-sequential decays, $N_{\rm ds}$, of sequential-sequential decays, $N_{\rm ss}$, of direct-random events, $N_{\rm dr}$ ("random" includes processes T_3, T_4, and T_5), of sequential-random decays, $N_{\rm sr}$, to obtain

$$C_b = \frac{N_{\rm dd} - N_{\rm ss} + \chi_0(N_{\rm dr} - N_{\rm sr})}{N_{\rm ls}} = 0.448 \pm 0.071, \quad (61)$$

where $N_{\rm ls}$ is the total number of like-sign dimuon events. This result agrees well with the value in Eq. (60). The uncertainty of this method is larger because of the small statistics of simulated like-sign dimuon events.

XIV. ASYMMETRY $A^b_{\rm sl}$

The uncorrected asymmetries a and A are obtained by counting the number of events of each charge in the inclusive muon and the like-sign dimuon samples, respectively. In total, there are 1.495×10^9 muons in the inclusive muon sample, and 3.731×10^6 events in the like-sign dimuon sample. We obtain

$$a = +0.009\,55 \pm 0.000\,03, \quad (62)$$

$$A = +0.005\,64 \pm 0.000\,53. \quad (63)$$

TABLE XIII. Sources of uncertainty on $A^b_{\rm sl}$ in Eqs. (64), (65), and (67). The first eight rows contain statistical uncertainties, and the next three rows contain systematic uncertainties.

Source	$\delta\sigma(A^b_{\rm sl})$ (64)	$\delta\sigma(A^b_{\rm sl})$ (65)	$\delta\sigma(A^b_{\rm sl})$ (67)
A or a (stat)	0.000 66	0.001 59	0.001 79
f_K or F_K (stat)	0.002 22	0.001 23	0.001 40
$P(\pi \to \mu)/P(K \to \mu)$	0.002 34	0.000 38	0.000 10
$P(p \to \mu)/P(K \to \mu)$	0.003 01	0.000 44	0.000 11
A_K	0.004 10	0.000 76	0.000 61
A_π	0.006 99	0.000 86	0.000 35
A_p	0.004 78	0.000 54	0.000 01
δ or Δ	0.004 05	0.001 05	0.000 77
f_K or F_K (syst)	0.021 37	0.003 00	0.001 28
π, K, p multiplicity	0.000 98	0.000 25	0.000 18
c_b or C_b	0.000 80	0.000 46	0.000 68
Total statistical	0.011 18	0.002 66	0.002 51
Total systematic	0.021 40	0.003 05	0.001 46
Total	0.024 15	0.004 05	0.002 90

The results obtained in Secs. V, VI, VII, VIII, IX, X, XI, XII, and XIII are used to calculate the asymmetries a_S and A_S from these values, which are then used to evaluate the charge asymmetry for semileptonic B-meson decays. The contributions of different background sources to the observed asymmetries a and A are summarized in Table XII.

The asymmetry $A^b_{\rm sl}$, extracted from the asymmetry a of the inclusive muon sample using Eqs. (9) and (52), is

$$A^b_{\rm sl} = +0.0094 \pm 0.0112\ (\text{stat}) \pm 0.0214\ (\text{syst}). \quad (64)$$

The contributions to the uncertainty on this value are given in Table XIII. Figure 14(a) shows a comparison of the asymmetry a and the background asymmetry $a_{\rm bkg} = f_S\delta + f_K a_K + f_\pi a_\pi + f_p a_p$, as a function of the muon p_T. There is excellent agreement between these two quantities, with the χ^2/d.o.f. for their difference being 2.4/5. Figure 14(b) shows the value of $f_S a_S = a - a_{\rm bkg}$, which is consistent with zero. The values a and $a_{\rm bkg}$ are given in Table XIV. This result agrees with expectations, since the value of the asymmetry a should be determined mainly by

TABLE XII. Contribution of different background sources to the observed asymmetry in the inclusive muon and like-sign dimuon samples. The last two lines give the asymmetries in the inclusive muon and like-sign dimuon samples before and after background subtraction. Only the statistical uncertainties are given.

Source	Inclusive muon	Like-sign dimuon
$(f_K a_K$ or $F_K A_K) \times 10^2$	$+0.854 \pm 0.018$	$+0.828 \pm 0.035$
$(f_\pi a_\pi$ or $F_\pi A_\pi) \times 10^2$	$+0.095 \pm 0.027$	$+0.095 \pm 0.025$
$(f_p a_p$ or $F_p A_p) \times 10^2$	$+0.012 \pm 0.022$	$+0.000 \pm 0.021$
$[(1 - f_{\rm bkg})\delta$ or $(2 - F_{\rm bkg})\Delta] \times 10^2$	-0.044 ± 0.016	-0.108 ± 0.037
$(a_{\rm bkg}$ or $A_{\rm bkg}) \times 10^2$	$+0.917 \pm 0.047$	$+0.816 \pm 0.070$
$(a$ or $A) \times 10^2$	$+0.955 \pm 0.003$	$+0.564 \pm 0.053$
$[(a - a_{\rm bkg})$ or $(A - A_{\rm bkg})] \times 10^2$	$+0.038 \pm 0.047$	-0.252 ± 0.088

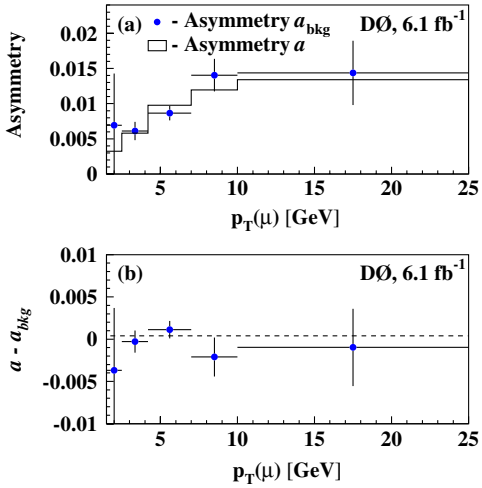

FIG. 14 (color online). (a) The asymmetry a_{bkg} (points with error bars) as expected from our measurements of the fractions and asymmetries of the background processes is compared to the measured asymmetry a of the inclusive muon sample (shown as histogram, since the statistical uncertainties are negligible). The asymmetry from CP violation is negligible compared to the background in the inclusive muon sample; (b) the difference $a - a_{\mathrm{bkg}}$. The horizontal dashed line shows the mean value of this difference.

the background, and the contribution from A_{sl}^b should be strongly suppressed by the small factor of $c_b = 0.070 \pm 0.006$.

The consistency of A_{sl}^b with zero in Eq. (64) and the good description of the charge asymmetry a for different values of the muon p_T shown in Fig. 14 constitute important tests of the validity of the background model and of the analysis method discussed in this article.

The second measurement of the asymmetry A_{sl}^b, obtained from the uncorrected asymmetry A of the like-sign dimuon sample using Eqs. (13), (52), and (53), is

$$A_{\mathrm{sl}}^b = -0.007\,36 \pm 0.002\,66\ (\mathrm{stat}) \pm 0.003\,05\ (\mathrm{syst}). \tag{65}$$

Here we take into account that both a_S and A_S in Eq. (13) are proportional to A_{sl}^b and that $F_{SS}C_b + F_{SL}c_b = 0.342 \pm 0.028$. The contributions to the uncertainty on A_{sl}^b for this measurement are also listed in Table XIII.

TABLE XIV. The measured asymmetry a and the expected background asymmetry a_{bkg} in the inclusive muon sample for different p_T bins. For the background asymmetry, the first uncertainty is statistical, and the second is systematic.

Bin	$a \times 10^2$	$a_{\mathrm{bkg}} \times 10^2$
0	0.324 ± 0.036	$0.693 \pm 0.379 \pm 0.632$
1	0.582 ± 0.007	$0.611 \pm 0.109 \pm 0.072$
2	0.978 ± 0.003	$0.865 \pm 0.054 \pm 0.088$
3	1.193 ± 0.008	$1.405 \pm 0.159 \pm 0.168$
4	1.339 ± 0.011	$1.438 \pm 0.206 \pm 0.408$

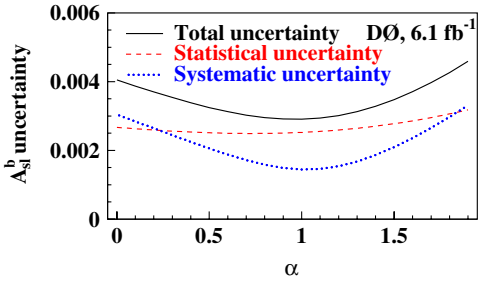

FIG. 15 (color online). Statistical (dashed line), systematic (dotted line), and total (full line) uncertainties on A_{sl}^b as a function of the parameter α of Eq. (66).

The results (64) and (65) represent two different measurements of A_{sl}^b. The uncertainties in Eq. (64) are much larger because the asymmetry a_s is divided by the small coefficient c_b. Since the same background processes contribute to the uncorrected asymmetries a and A, their uncertainties in Eqs. (64) and (65) are strongly correlated. We take advantage of this correlation to obtain a single optimized value of A_{sl}^b, with higher precision, using a linear combination of the uncorrected asymmetries

$$A' \equiv A - \alpha a, \tag{66}$$

and choosing the coefficient α in order to minimize the total uncertainty on the value of A_{sl}^b.

It is shown in Secs. V, VI, VII, VIII, IX, X, XI, and XII that the contributions from background sources in Eqs. (9) and (13) are of the same order of magnitude. On the other hand, the dependence of A and a on the asymmetry A_{sl}^b, according to Eqs. (55) and (60), is significantly different, with $C_b \gg c_b$. As a result, we can expect a reduction of background uncertainties in (66) for $\alpha \approx 1$ with a limited reduction of the statistical sensitivity on A_{sl}^b. Figure 15 shows the statistical, systematic, and total uncertainties on A_{sl}^b as a function of the parameter α. The total uncertainty on A_{sl}^b has a minimum for $\alpha = 0.959$, and the corresponding value of the asymmetry A_{sl}^b is

$$A_{\mathrm{sl}}^b = -0.009\,57 \pm 0.002\,51\ (\mathrm{stat}) \pm 0.001\,46\ (\mathrm{syst}). \tag{67}$$

This value is our final result for A_{sl}^b. It differs by 3.2 standard deviations from the standard model prediction of A_{sl}^b given in Eq. (4). The different contributions to the total uncertainty of A_{sl}^b in Eq. (67) are listed in Table XIII.

XV. CONSISTENCY CHECKS

To check the stability of the result, we repeat this measurement with modified selections, or with subsets of the available data sample. Changes are implemented in a variety of tests:

(i) Test A: Using only the part of the data sample corresponding to the first 2.8 fb^{-1}.
(ii) Test B: In addition to the reference selections, requiring at least three hits in muon wire chamber layers B or C, and the χ^2 for a fit to a track segment reconstructed in the muon detector to be less than 8.
(iii) Test C: Since the background muons are produced by decays of kaons and pions, their track parameters measured by the central tracker and by the muon system are different. Therefore, the fraction of background strongly depends on the χ^2 of the difference between these two measurements. The requirement on this χ^2 is changed from 40 to 4 in this study.
(iv) Test D: The maximum value of the transverse impact parameter is changed from 0.3 to 0.05 cm, and the requirement on the longitudinal distance between the point of closest approach to the beam and the associated interaction vertex is changed from 0.5 to 0.05 cm. This test serves also as a cross-check against the possible contamination from muons from cosmic rays in the selected sample.
(v) Test E: Using only low-luminosity events with fewer than three interaction vertices.
(vi) Test F: Using only events corresponding to two of the four possible configurations of the magnets, for which the solenoid and toroid polarities are identical.
(vii) Test G: Changing the requirement on the invariant mass of the two muons from 2.8 to 12 GeV.
(viii) Test H: Using the same muon p_T requirement, $p_T > 4.2$ GeV, over the full detector acceptance.
(ix) Test I: Requiring the muon p_T to be <7.0 GeV.
(x) Test J: Requiring the azimuthal angle ϕ of the muon track to be in the range $0 < \phi < 4$ or $5.7 < \phi < 2\pi$. This selection excludes muons directed to the region of poor muon identification efficiency in the support structure of the detector.
(xi) Test K: Requiring the muon η to be in the range $|\eta| < 1.6$ (this test serves also as a cross-check against the possible contamination from muons associated with the beam halo).
(xii) Test L: Requiring the muon η to be in the range $|\eta| < 1.2$ or $1.6 < |\eta| < 2.2$.
(xiii) Test M: Requiring the muon η to be in the range $|\eta| < 0.7$ or $1.2 < |\eta| < 2.2$.
(xiv) Test N: Requiring the muon η to be in the range $0.7 < |\eta| < 2.2$.
(xv) Test O: Using like-sign dimuon events passing at least one single muon trigger, while ignoring the requirement of a dimuon trigger for these events.
(xvi) Test P: Using like-sign dimuon events passing both single muon and dimuon triggers.
(xvii) Test Q: Using the events collected when the muon detector is fully operational.

A summary of the results from these studies is presented in Tables XV and XVI. The last line, denoted as "significance," gives the difference between the reference result (column Ref.) and each modification, divided by its uncertainty, and taking into account the overlap between the samples. The statistical uncertainties are used in the calculation of the significance of the difference between two results. These tests demonstrate an impressive stability of the A^b_{sl} result, and provide a strong confirmation of the validity of the method. As a result of the variations of the selection criteria, all input quantities are changed over a wide range, while the asymmetry A^b_{sl} remains well within the assigned uncertainties. For example, the uncorrected asymmetry A changes by a factor ≈ 1.5 in test C, while the asymmetry A^b_{sl} changes by less than 7%. It should also be noted that reducing the kaon background in test C yields a negative asymmetry A.

Figure 16 shows the observed and expected uncorrected like-sign dimuon charge asymmetry as a function of the dimuon invariant mass. The expected asymmetry is computed using Eq. (13) and all the measurements of the sample composition and of the asymmetries. We compare the expected uncorrected asymmetry using two different assumptions for A^b_{sl}. In Fig. 16(a) the observed asymmetry is compared to the expectation for $A^b_{\text{sl}} = 0$, while Fig. 16(b) shows the expected asymmetry for $A^b_{\text{sl}} = -0.009\,57$. A possible systematic discrepancy between the observed and expected asymmetries can be observed for $A^b_{\text{sl}} = 0$,

TABLE XV. Measured asymmetry A^b_{sl} with reference selections (column Ref.) and variations A–H.

	Ref.	A	B	C	D	E	F	G	H
$N(\mu\mu) \times 10^{-6}$	3.731	1.809	2.733	1.809	1.785	2.121	1.932	1.736	1.783
$a \times 10^2$	+0.955	+0.988	+0.791	+0.336	+1.057	+0.950	+1.029	+0.955	+1.032
$A \times 10^2$	+0.564	+0.531	+0.276	−0.229	+0.845	+0.543	+0.581	+0.821	+0.632
α	0.959	0.901	0.942	1.089	1.083	0.902	0.915	1.029	0.877
$[(2 - F_{\text{bkg}})\Delta - \alpha f_S \delta] \times 10^2$	−0.065	−0.072	−0.143	−0.200	−0.074	−0.075	−0.069	−0.023	−0.061
F_{bkg}	0.409	0.372	0.401	0.303	0.384	0.385	0.426	0.449	0.343
$A^b_{\text{sl}} \times 10^2$	−0.957	−0.976	−1.084	−0.892	−1.107	−0.888	−1.096	−0.873	−0.769
$\sigma(A^b_{\text{sl}}) \times 10^2$ (stat)	0.251	0.330	0.293	0.315	0.402	0.328	0.375	0.388	0.336
Significance		0.090	0.846	0.324	0.478	0.326	0.498	0.281	0.779

TABLE XVI. Measured asymmetry $A^b_{\rm sl}$ with reference selections (column Ref.) and variations I–Q.

	Ref	I	J	K	L	M	N	O	P	Q
$N(\mu\mu) \times 10^{-6}$	3.731	2.569	2.208	1.884	1.909	2.534	2.122	2.002	1.772	2.723
$a \times 10^2$	+0.955	+0.896	+1.002	+0.984	+1.098	+0.679	+1.097	+0.968	+0.968	+0.979
$A \times 10^2$	+0.564	+0.407	+0.648	+0.576	+0.630	+0.353	+0.748	+0.722	+0.692	+0.643
α	0.959	0.975	0.913	0.895	0.877	0.940	0.949	0.983	0.934	0.934
$[(2 - F_{\rm bkg})\Delta - \alpha f_S \delta] \times 10^2$	−0.065	−0.101	−0.079	−0.125	−0.142	−0.081	−0.019	−0.046	−0.044	−0.059
$F_{\rm bkg}$	0.409	0.439	0.412	0.363	0.365	0.412	0.452	0.419	0.398	0.420
$A^b_{\rm sl} \times 10^2$	−0.957	−1.295	−0.710	−0.851	−0.801	−0.759	−1.102	−0.897	−0.833	−0.860
$\sigma(A^b_{\rm sl}) \times 10^2$ (stat)	0.251	0.314	0.320	0.320	0.383	0.275	0.344	0.346	0.349	0.302
Significance		1.798	1.241	0.482	0.539	1.317	0.622	0.240	0.485	0.577

while it essentially disappears for the measured $A^b_{\rm sl}$ value corresponding to Eq. (67). It can also be seen that the observed asymmetry changes as a function of the dimuon invariant mass, and that the expected asymmetry reproduces this effect when $A^b_{\rm sl} = -0.009\,57$. This dependence of the asymmetry on the invariant mass of the muon pair is a complex function of the production mechanism, of the mass of the particles being produced, and of their decays. The agreement between the observed and expected asymmetries indicates that the physics leading to the observed asymmetry is well described by the contributions from the backgrounds and from decaying b hadrons.

We conclude that our method of analysis provides a consistent description of the dimuon charge asymmetry for a wide range of input parameters, even for significantly modified selection criteria.

In addition to the described consistency checks, we perform other studies to verify the validity of the analysis method. These tests are described in Appendixes C, D, and E. We determine the asymmetry of track reconstruction and the asymmetry of trigger selection. We also measure the ratio F_K/f_K using an alternative fitting procedure. These studies do not show any bias in the extracted value of $A^b_{\rm sl}$.

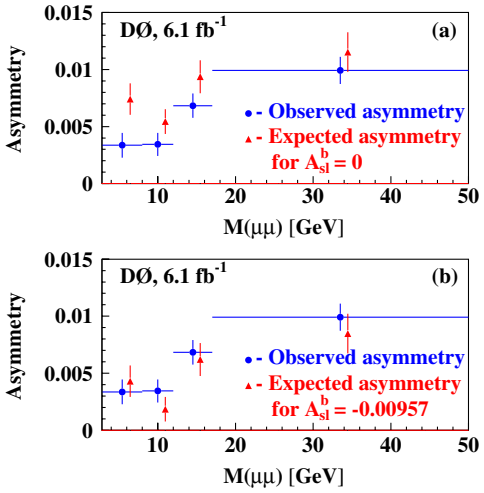

FIG. 16 (color online). The observed and expected like-sign dimuon charge asymmetries in bins of dimuon invariant mass. The expected asymmetry is shown for (a) $A^b_{\rm sl} = 0.0$ and (b) $A^b_{\rm sl} = -0.009\,57$.

XVI. COMPARISON WITH EXISTING MEASUREMENTS

The measured value of $A^b_{\rm sl}$ places a constraint on the charge asymmetries of semileptonic decays of B^0_d and B^0_s mesons, and the CP-violating phases of the B^0_d and B^0_s mass mixing matrices. Calculating the coefficients in Eq. (A9) assuming the current PDG values [2] for all parameters (details are given in Appendix A), we obtain

$$A^b_{\rm sl} = (0.506 \pm 0.043)a^d_{\rm sl} + (0.494 \pm 0.043)a^s_{\rm sl}. \quad (68)$$

Figure 17 presents this measurement in the $a^d_{\rm sl} - a^s_{\rm sl}$ plane, together with the existing direct measurements of $a^d_{\rm sl}$ from the B factories [24] and of our independent measurement of $a^s_{\rm sl}$ in $B^0_s \to D_s \mu X$ decays [25]. Using Eqs. (67) and (68) and the current experimental value of $a^d_{\rm sl} = -0.0047 \pm 0.0046$ [24], we obtain

$$a^s_{\rm sl} = -0.0146 \pm 0.0075. \quad (69)$$

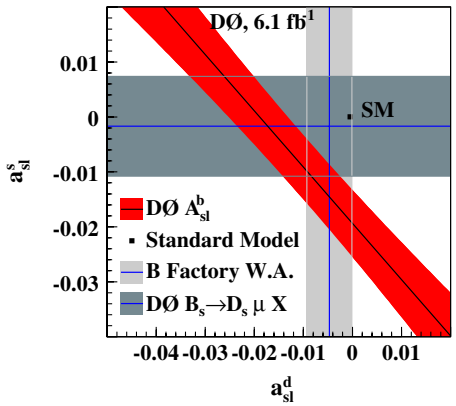

FIG. 17 (color online). Comparison of $A^b_{\rm sl}$ in data with the standard model prediction for $a^d_{\rm sl}$ and $a^s_{\rm sl}$. Also shown are the existing measurements of $a^d_{\rm sl}$ [24] and $a^s_{\rm sl}$ [25]. The error bands represent the ± 1 standard deviation uncertainties on each individual measurement.

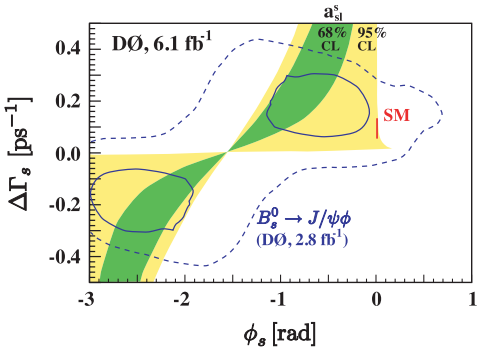

FIG. 18 (color online). The 68% and 95% C.L. regions of probability for $\Delta\Gamma_s$ and ϕ_s values obtained from this measurement, considering the experimental constraints on a^d_{sl} [24]. The solid and dashed curves show, respectively, the 68% and 95% C.L. contours from the $B^0_s \to J/\psi\phi$ measurement [26]. Also shown is the standard model (SM) prediction for ϕ_s and $\Delta\Gamma_s$.

This agrees with our direct measurement of $a^s_{sl} = -0.0017 \pm 0.0091$ [25].

An independent method for measuring ϕ_s is through $B^0_s \to J/\psi\phi$ decays. Such measurements have been performed by the D0 [26] and CDF [27] Collaborations. All measurements are consistent and the combined value of ϕ_s differs from the standard model prediction by about 2 standard deviations [28].

Taking into account the experimental constraints on a^d_{sl} [24], Fig. 18 shows the 68% and 95% C.L. regions of $\Delta\Gamma_s$ and ϕ_s obtained from our measurement. The 68% and 95% C.L. regions from the D0 measurement using the $B^0_s \to J/\psi\phi$ decay [26] are also included in this figure. Since the sign of $\Delta\Gamma_s$ is not known, there is also a mirror solution with $\phi_s \to -\pi - \phi_s$, corresponding to the change $\Delta\Gamma_s \to -\Delta\Gamma_s$. It can be seen that the D0 results are consistent. Figure 19 shows the probability contours in the $(\phi_s, \Delta\Gamma_s)$ plane for the combination of our measurement with the result of Ref. [26].

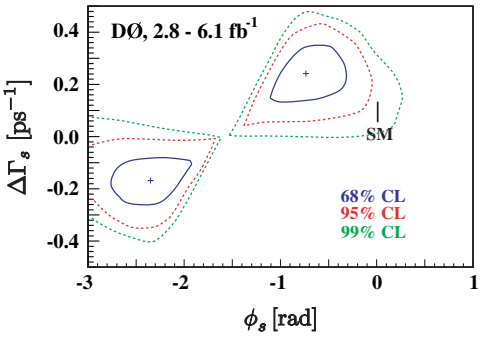

FIG. 19 (color online). Probability contours in the $(\phi_s, \Delta\Gamma_s)$ plane for the combination of this measurement with the result of Ref. [26], using the experimental constraints on a^d_{sl} [24].

XVII. CONCLUSIONS

We have measured the like-sign dimuon charge asymmetry A^b_{sl} of semileptonic b-hadron decays:

$$A^b_{sl} = -0.009\,57 \pm 0.002\,51\ (\text{stat}) \pm 0.001\,46\ (\text{syst}). \tag{70}$$

This measurement is obtained from a data set corresponding to 6.1 fb^{-1} of integrated luminosity collected with the D0 detector at the Fermilab Tevatron collider. It is consistent with our previous measurement [17] obtained with 1 fb^{-1} and supersedes it. This asymmetry is in disagreement with the prediction of the standard model by 3.2 standard deviations. This is the first evidence for anomalous CP violation in the mixing of neutral B mesons.

ACKNOWLEDGMENTS

We thank the staffs at Fermilab and collaborating institutions, and acknowledge support from the DOE and NSF (USA); CEA and CNRS/IN2P3 (France); FASI, Rosatom, and RFBR (Russia); CNPq, FAPERJ, FAPESP, and FUNDUNESP (Brazil); DAE and DST (India); Colciencias (Colombia); CONACyT (Mexico); KRF and KOSEF (Korea); CONICET and UBACyT (Argentina); FOM (The Netherlands); STFC and the Royal Society (United Kingdom); MSMT and GACR (Czech Republic); CRC Program and NSERC (Canada); BMBF and DFG (Germany); SFI (Ireland); The Swedish Research Council (Sweden); and CAS and CNSF (China).

APPENDIX A: THEORY

This Appendix is included for completeness and to define the notations. Assuming CPT symmetry, the mixing and decay of the B^0_q, $\bar{B}^0_q$ pair ($q = s, d$) is described [29] by

$$i\frac{d}{dt}\begin{pmatrix} B^0_q(t) \\ \bar{B}^0_q(t) \end{pmatrix} = \left(\begin{bmatrix} M_q & M^{12}_q \\ (M^{12}_q)^* & M_q \end{bmatrix} - \frac{i}{2}\begin{bmatrix} \Gamma_q & \Gamma^{12}_q \\ (\Gamma^{12}_q)^* & \Gamma_q \end{bmatrix}\right) \cdot \begin{pmatrix} B^0_q(t) \\ \bar{B}^0_q(t) \end{pmatrix}, \tag{A1}$$

where M_q, M^{12}_q, Γ_q, and Γ^{12}_q are the elements of the mass matrix of the $B^0_q\bar{B}^0_q$ system. The matrix element M^{12}_q is due to box diagrams [2]. New particles foreseen in extensions of the standard model can contribute to these box diagrams, and physics beyond the standard model can therefore modify the phase and amplitude of M^{12}_q.

The eigenvalues of the mass matrix in Eq. (A1) are

$$M_q + \frac{1}{2}\Delta M_q - \frac{i}{2}\left(\Gamma_q - \frac{1}{2}\Delta\Gamma_q\right), \tag{A2}$$

$$M_q - \frac{1}{2}\Delta M_q - \frac{i}{2}\left(\Gamma_q + \frac{1}{2}\Delta\Gamma_q\right), \tag{A3}$$

where, by definition, $\Delta M_q > 0$. Notice the sign conven-

tions for ΔM_q and $\Delta\Gamma_q$. With this convention, $\Delta\Gamma_q$ is positive in the standard model. A violation of the CP symmetry is caused by a nonzero value of the phase

$$\phi_q \equiv \arg\left(-\frac{M_q^{12}}{\Gamma_q^{12}}\right). \tag{A4}$$

The observable quantities are M_q, Γ_q, ΔM_q, $\Delta\Gamma_q$, and ϕ_q, with

$$\Delta M_q = 2|M_q^{12}|, \qquad \Delta\Gamma_q = 2|\Gamma_q^{12}|\cos\phi_q. \tag{A5}$$

The charge asymmetry $a_{\rm sl}^q$ for "wrong-charge" semileptonic B_q^0-meson decay induced by oscillations is defined as

$$a_{\rm sl}^q = \frac{\Gamma(\bar{B}_q^0(t) \to \mu^+ X) - \Gamma(B_q^0(t) \to \mu^- X)}{\Gamma(\bar{B}_q^0(t) \to \mu^+ X) + \Gamma(B_q^0(t) \to \mu^- X)}. \tag{A6}$$

This quantity is independent of the decay time t, and can be expressed as

$$a_{\rm sl}^q = \frac{|\Gamma_q^{12}|}{|M_q^{12}|}\sin\phi_q = \frac{\Delta\Gamma_q}{\Delta M_q}\tan\phi_q. \tag{A7}$$

The like-sign dimuon charge asymmetry $A_{\rm sl}^b$ for semileptonic decays of b hadrons produced in proton-antiproton ($p\bar{p}$) collisions is defined as

$$A_{\rm sl}^b \equiv \frac{N_b^{++} - N_b^{--}}{N_b^{++} + N_b^{--}}, \tag{A8}$$

where N_b^{++} and N_b^{--} are the numbers of events containing two b hadrons that decay semileptonically, producing two positive or two negative muons, respectively, with only the direct semileptonic decays $b \to \mu X$ considered in the definition of N_b^{++} and N_b^{--}. The asymmetry $A_{\rm sl}^b$ can be expressed [12] as

$$A_{\rm sl}^b = \frac{f_d Z_d a_{\rm sl}^d + f_s Z_s a_{\rm sl}^s}{f_d Z_d + f_s Z_s}, \tag{A9}$$

where

$$Z_q \equiv \frac{1}{1 - y_q^2} - \frac{1}{1 + x_q^2}, \tag{A10}$$

$$y_q \equiv \frac{\Delta\Gamma_q}{2\Gamma_q}, \tag{A11}$$

$$x_q \equiv \frac{\Delta M_q}{\Gamma_q}, \tag{A12}$$

with $q = d, s$. The quantities f_d and f_s are the production fractions for $\bar{b} \to B_d^0$ and $\bar{b} \to B_s^0$, respectively. These fractions have been measured for $p\bar{p}$ collisions at the Tevatron [2]:

$$f_d = 0.323 \pm 0.037, \qquad f_s = 0.118 \pm 0.015. \tag{A13}$$

All other parameters in (A9) are also taken from Ref. [2]:

$$\begin{aligned} x_d &= 0.774 \pm 0.008, \qquad & y_d &= 0, \\ x_s &= 26.2 \pm 0.5, \qquad & y_s &= 0.046 \pm 0.027. \end{aligned} \tag{A14}$$

Substituting these values in Eq. (A9), we obtain

$$A_{\rm sl}^b = (0.506 \pm 0.043)a_{\rm sl}^d + (0.494 \pm 0.043)a_{\rm sl}^s. \tag{A15}$$

Using the values of $a_{\rm sl}^d$, $a_{\rm sl}^s$ from Ref. [1],

$$\begin{aligned} a_{\rm sl}^d({\rm SM}) &= (-4.8^{+1.0}_{-1.2}) \times 10^{-4} \\ a_{\rm sl}^s({\rm SM}) &= (2.1 \pm 0.6) \times 10^{-5}, \end{aligned} \tag{A16}$$

the predicted value of $A_{\rm sl}^b$ in the standard model is

$$A_{\rm sl}^b({\rm SM}) = (-2.3^{+0.5}_{-0.6}) \times 10^{-4}. \tag{A17}$$

The current experimental values of the two semileptonic asymmetries are $a_{\rm sl}^d = -0.0047 \pm 0.0046$ [24] and $a_{\rm sl}^s = -0.0017 \pm 0.0091$ [25].

It can be concluded from Eq. (A17) that the standard model predicts a small negative value of $A_{\rm sl}^b$ with rather small uncertainty. Any significant deviation of $A_{\rm sl}^b$ from the SM prediction on a scale larger than that of the uncertainty on $A_{\rm sl}^b$ would be an unambiguous signal of new physics.

The asymmetry $A_{\rm sl}^b$ is also equivalent to the charge asymmetry of semileptonic decays of b hadrons to wrong-charge muons that are induced by oscillations [12], i.e.,

$$a_{\rm sl}^b \equiv \frac{\Gamma(\bar{B} \to \mu^+ X) - \Gamma(B \to \mu^- X)}{\Gamma(\bar{B} \to \mu^+ X) + \Gamma(B \to \mu^- X)} = A_{\rm sl}^b. \tag{A18}$$

Without initial flavor tagging it is impossible to correctly select the decays producing a muon of wrong charge from a sample of semileptonic decays of b quarks. The charge asymmetry of semileptonic b hadron decays, contrary to the charge asymmetry of like-sign dimuons, is therefore reduced by the contribution of decays producing a muon with "correct" charge, and is consequently less sensitive to the asymmetry $A_{\rm sl}^b$.

New physical phenomena can change the phase and magnitude of the standard model $M_s^{12,{\rm SM}}$ to

$$M_s^{12} \equiv M_s^{12,{\rm SM}} \cdot \Delta_s = M_s^{12,{\rm SM}} \cdot |\Delta_s| e^{i\phi_s^\Delta}, \tag{A19}$$

where

$$\phi_s = \phi_s^{\rm SM} + \phi_s^\Delta, \qquad \phi_s^{\rm SM} = 0.0042 \pm 0.0014. \tag{A20}$$

Other changes expected as a result of new sources of CP violation [1] are

$$\Delta M_s = \Delta M_s^{\rm SM} \cdot |\Delta_s| = (19.30 \pm 6.74)\ {\rm ps}^{-1} \cdot |\Delta_s|, \tag{A21}$$

$$\Delta\Gamma_s = 2|\Gamma_s^{12}|\cos\phi_s = (0.096 \pm 0.039)\ {\rm ps}^{-1} \cdot \cos\phi_s, \tag{A22}$$

$$\frac{\Delta\Gamma_s}{\Delta M_s} = \frac{|\Gamma_s^{12}|}{|M_s^{12,\mathrm{SM}}|}\cdot\frac{\cos\phi_s}{|\Delta_s|} = (4.97 \pm 0.94)\cdot 10^{-3}\cdot\frac{\cos\phi_s}{|\Delta_s|}, \quad \text{(A23)}$$

$$a_{\mathrm{sl}}^s = \frac{|\Gamma_s^{12}|}{|M_s^{12,\mathrm{SM}}|}\cdot\frac{\sin\phi_s}{|\Delta_s|} = (4.97 \pm 0.94)\cdot 10^{-3}\cdot\frac{\sin\phi_s}{|\Delta_s|}. \quad \text{(A24)}$$

The $B_s^0 \to J/\psi\phi$ decay can also be used to investigate CP violation. In that case, the CP-violating phase obtained from fits to the $B_s^0 \to J/\psi\phi$ angular distributions is modified as follows [1]:

$$\phi_s^{J/\psi\phi} = -2\beta_s^{\mathrm{SM}} + \phi_s^{\Delta}, \quad \text{(A25)}$$

where

$$\beta_s^{\mathrm{SM}} = \arg[-V_{ts}V_{tb}^*/(V_{cs}V_{cb}^*)] = 0.019 \pm 0.001 \quad \text{(A26)}$$

and the quantities V_{ts}, V_{tb}, V_{cs}, and V_{cb} are the parameters of the Cabibbo-Kobayashi-Maskawa matrix. The contributions of new physics to ϕ_s and $\phi_s^{J/\psi\phi}$ are identical.

APPENDIX B: RECONSTRUCTION OF EXCLUSIVE DECAYS

1. Reconstruction of K_S mesons

The K_S meson is used to reconstruct the K^{*+} meson [13] and to measure the fraction and asymmetry of $\pi \to \mu$ tracks. The $K_S \to \pi^+\pi^-$ decay is reconstructed by requiring two tracks with opposite charge. Each track must have an impact parameter significance with respect to the interaction vertex > 3, where the significance is defined as $\sqrt{[\epsilon_T/\sigma(\epsilon_T)]^2 + [\epsilon_L/\sigma(\epsilon_L)]^2}$, and ϵ_T (ϵ_L) is the projection of the track impact parameter on the plane transverse to the beam direction (along the beam direction), and $\sigma(\epsilon_T) \times [\sigma(\epsilon_L)]$ is its uncertainty. At least one of the tracks must have an impact parameter significance >4, and at least one of the particles must have $p_T > 1.5$ GeV. The two tracks must share a common vertex that is separated from the primary interaction point by more than 4 mm in the transverse plane. The significance of the reconstructed impact parameter for the K_S must be <4. All K_S candidates satisfying these selection criteria are used to reconstruct the $K^{*+} \to K_S\pi^+$ decay. In addition, for the measurement of the fraction and asymmetry of $\pi \to \mu$ tracks, we require that one of the pions from K_S decay pass the muon selection given in Sec. III.

Figure 20 displays the $\pi^+\pi^-$ invariant mass distribution of $K_S \to \pi^+\pi^-$ candidates in the inclusive muon sample for all $\pi \to \mu$ with $7.0 < p_T < 10.0$ GeV. We show separately the sum and the difference of the distributions for the samples with positive and negative $\pi \to \mu$ tracks, which are used to measure the asymmetry of $\pi \to \mu$ tracks. The

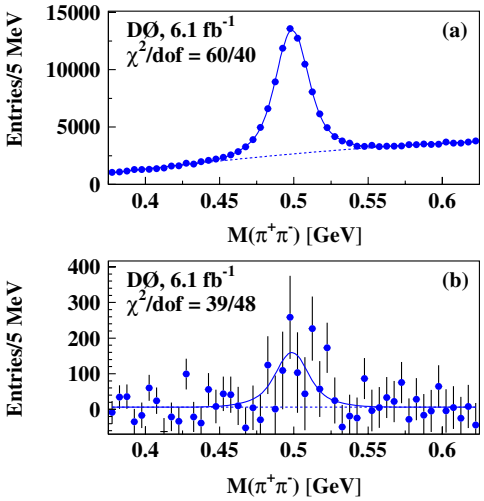

FIG. 20 (color online). The $\pi^+\pi^-$ invariant mass distribution of K_S candidates in the inclusive muon sample for $\pi \to \mu$ with $7.0 < p_T < 10.0$ GeV. (a) The sum of the distributions for positive and negative $\pi \to \mu$ tracks and (b) their difference. The solid lines present the result of the fit; the dashed lines show the background contribution.

K_S signal is fitted with a double Gaussian, and the background is parametrized by a third degree polynomial for the sum of the two distributions and a straight line for their difference. While fitting the difference of the distributions all the parameters describing the K_S signal, except its normalization, are fixed to the values obtained from the fit to the sum of the distributions.

2. Reconstruction of K^{*+} mesons

The K^{*+} [13] signal is obtained by combining the reconstructed K_S meson with an additional track which is assigned the mass of the charged pion. The K_S candidate must satisfy the track selection criteria given in Sec. III, except for the requirements on the number of hits in the tracking detectors and the χ^2 of the track fit. The invariant mass of the $\pi^+\pi^-$ system must be $480 < M(\pi^+\pi^-) < 515$ MeV. The additional track must have at least 2 axial and 1 stereo hits in the silicon microstrip detector, at least 3 axial and 3 stereo hits in the fiber tracker, and a track impact parameter significance <3 relative to the interaction vertex. The cosine of the angle between the direction of the K_S meson and the additional track must be greater than 0.3. The K_S and the additional track must be consistent with sharing the same interaction vertex.

Figure 21 shows the $K_S\pi^+$ invariant mass distribution. The K^{*+} signal is fitted with a relativistic Breit-Wigner function convoluted with a Gaussian resolution, and the background is parametrized by the function

$$f_{\mathrm{bkg}}(M) = (M - M_K - M_\pi)^{p_0}\exp(p_1 M + p_2 M^2 + p_3 M^3), \quad \text{(B1)}$$

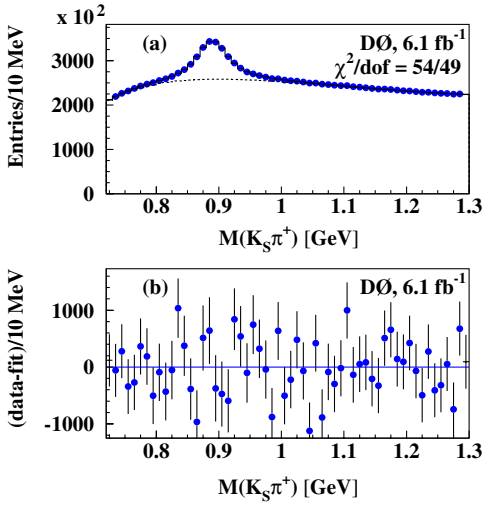

FIG. 21 (color online). (a) The $K_S\pi^+$ invariant mass distribution of K^{*+} candidates in the inclusive muon sample. The solid line presents the result of the fit; the dashed line shows the background contribution. (b) The difference between data and the fit result.

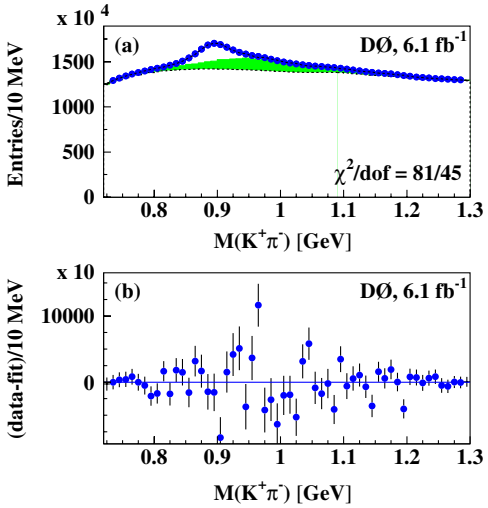

FIG. 22 (color online). (a) The $K^+\pi^-$ invariant mass distribution of K^{*0} candidates in the inclusive muon sample. The solid line corresponds to the result of the fit and the dashed line shows the contribution from the combinatorial background. The shaded histogram is the contribution of $\rho^0 \to \pi^+\pi^-$ events. (b) The difference between data and the result of the fit.

which includes a threshold factor. Here M is the $K_S\pi^+$ invariant mass, and p_0, p_1, p_2, and p_3 are free parameters. Figure 21(b), which shows the difference between data points and the result of the fit, demonstrates the good quality of the fit with $\chi^2/\text{d.o.f.} = 54/49$. The measured width of the K^{*+} meson is $\Gamma(K^{*+}) = 47.9 \pm 1.4(\text{stat})$ MeV, which is consistent with the current PDG value [2].

3. Reconstruction of K^{*0} mesons

The K^{*0} meson is reconstructed by selecting two tracks of opposite charge and assigning one of them the mass of the charged kaon. This particle is required to be identified as a muon and to pass the muon selection criteria given in Sec. III. The second track is assigned the mass of a pion and required to satisfy the criteria used to select the pion in the $K^{*\pm}$ reconstruction.

Figure 22 shows the $K^+\pi^-$ [13] invariant mass distribution of the K^{*0} candidates with $K \to \mu$ in the inclusive muon sample, while Fig. 23 shows the corresponding mass distribution in the like-sign dimuon sample.

The measurement of the number of $K^{*0} \to K^+\pi^-$ decays with $K \to \mu$ is complicated because of the large combinatorial background under the K^{*0} signal, and because of the contribution of light meson resonances decaying to $\pi^+\pi^-$. The most important contribution comes from the $\rho^0 \to \pi^+\pi^-$ decay with $\pi \to \mu$. It produces a peak in the mass region close to the K^{*0} mass. Figure 24 shows the mass distribution of simulated $\rho^0 \to \pi^+\pi^-$ decays with one pion assigned the kaon mass. This pion is also required to satisfy the track selections.

To overcome these misidentification difficulties, the fit to the $K^+\pi^-$ mass distribution is performed in several steps, assuming for the width of the K^{*0} meson the value obtained in the previous section for the K^{*+} meson. Contrary to the $K^+\pi^-$ system, the decays of light resonances do not contribute into the $K_S\pi^+$ mass distribution because the K_S meson is identified unambiguously, and the K^{*+} signal is clean and unbiased.

The K^{*0} mass and detector resolution for $K^{*0} \to K^+\pi^-$ with $K \to \mu$ are obtained from a fit to the difference of the $K^+\pi^-$ and $K^-\pi^+$ mass distributions. The reconstruction

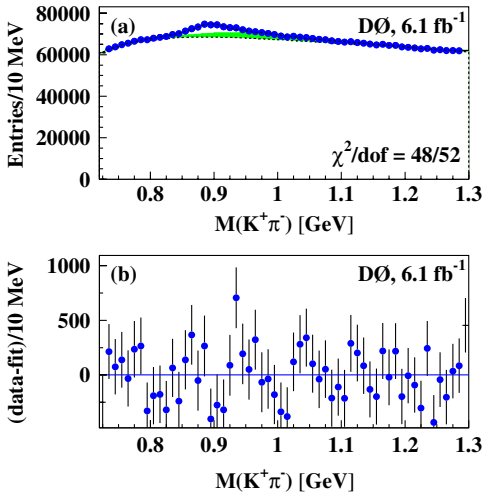

FIG. 23 (color online). (a) The $K^+\pi^-$ invariant mass distribution of K^{*0} candidates in the like-sign dimuon sample. The solid line corresponds to the result of the fit and the dashed line shows the contribution from the combinatorial background. The shaded histogram is the contribution of $\rho^0 \to \pi^+\pi^-$ events. (b) The difference between data and the result of the fit.

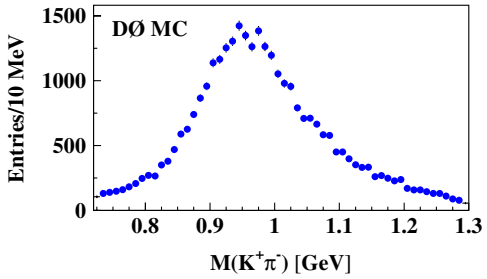

FIG. 24 (color online). The $K^+\pi^-$ invariant mass distribution of simulated $\rho^0 \to \pi^+\pi^-$ decays, where the mass of the charged kaon is assigned to one of the two reconstructed tracks.

efficiency of $K \to \mu$ tracks demonstrates a charge asymmetry $\approx 6\%$ (see Sec. XI). Such an asymmetry is significantly smaller for $\pi \to \mu$ tracks, and the contribution of $\rho \to \pi^+\pi^-$ and other light resonances is therefore suppressed in the difference of the $K^+\pi^-$ and $K^-\pi^+$ mass distributions. In addition, the contribution of the combinatorial background is significantly reduced, as can be seen in Fig. 25(a). The K^{*0} signal is fitted with a relativistic Breit-Wigner function convoluted with a Gaussian resolution, and the background is parametrized by the function (B1). Figure 25(b), which shows the difference between data and the result of the fit, indicates a moderate quality for the fit, with $\chi^2/\text{d.o.f.} = 71/52$. The fit gives $\sigma(M) = 12.2 \pm 1.5(\text{stat})$ MeV for the K^{*0} mass resolution of the detector. The mass difference between K^{*0} and K^{*+} is

$$M(K^{*0}) - M(K^{*+}) = 3.50 \pm 0.66\ (\text{stat})\ \text{MeV}, \quad \text{(B2)}$$

which is consistent with the PDG value of 4.34 ± 0.36 MeV [2].

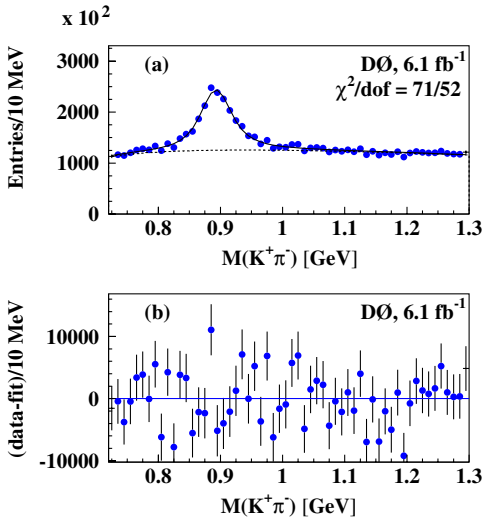

FIG. 25 (color online). (a) The difference of the $K^+\pi^-$ and $K^-\pi^+$ mass distributions of K^{*0} candidates in the inclusive muon sample. The solid line represents the result of the fit, while the dashed line shows the background contribution. (b) The difference between data and the result of the fit.

The number of K^{*0} events in the inclusive muon and in the like-sign dimuon samples is determined from the fit of the mass distributions shown in Figs. 22 and 23. The signal is parametrized with the convolution of a relativistic Breit-Wigner function and a Gaussian resolution. The K^{*0} mass and width and the detector resolution are fixed in the fit to the values obtained from the fit to the distribution in Fig. 25(a). The mass distribution of the $\rho^0 \to \pi^+\pi^-$ background is taken from the MC simulation. To improve the quality of the fit, the parametrization of the background is modified by adding two additional Gaussian terms:

$$f'_{\text{bkg}}(M) = f_{\text{bkg}}(M) + p_4 \exp\left(-\frac{(M - M_1)^2}{2\sigma_1^2}\right) + p_5 \exp\left(-\frac{(M - M_2)^2}{2\sigma_2^2}\right). \quad \text{(B3)}$$

Here $f_{\text{bkg}}(M)$ is given in (B1). The additional terms are needed to describe the distortion of the smooth behavior of the combinatorial background at large masses of $M \approx 1.15$ GeV, due to the contributions of other light resonances, and should be considered as a parametrization of the observed mass distribution rather than the contribution from specific sources. These terms are significant only because of the large statistics of the inclusive muon sample, which contains about 10^7 entries per bin in Fig. 22. The fit of the K^{*0} signal in the like-sign dimuon sample is of the same quality without these additional terms. The results do not change significantly if these terms are omitted. The impact of these terms on the final measurement is included in the systematic uncertainties of the fractions f_K and F_K discussed in Sec. VIII.

In the fit to the inclusive muon distribution, the parameters M_1, M_2, σ_1, and σ_2 and the contribution of $\rho^0 \to \pi^+\pi^-$ are allowed to vary. The ratio of the fractions of ρ^0 and K^{*0} mesons is constrained within 10% of the value obtained in the simulation. The fit yields $M_1 = 1.095 \pm 0.005$ GeV and $M_2 = 1.170 \pm 0.007$ GeV, which is far from the region of the K^{*0} mass, and does not influence the fitted number of K^{*0} mesons. The $\chi^2/\text{d.o.f.}$ of the fit is $81/45$. The results of the fit and corresponding residuals are shown in Fig. 22.

In the fit to the like-sign dimuon distribution the parameters M_1, M_2, σ_1, and σ_2 are fixed to the values obtained in the fit of the inclusive muon sample. The $\chi^2/\text{d.o.f.}$ of the fit is $48/52$. The results of the fit and corresponding residuals are shown in Fig. 23.

4. Reconstruction of $\phi(1020)$ mesons

The $\phi(1020)$ meson is reconstructed by selecting two tracks with opposite charge and assigning both of them the mass of the charged kaon. One track is required to pass the track selections of Sec. III. The second one satisfies the same selection criteria as the pion in the $K^{*\pm}$ and K^{*0} reconstructions.

Figure 26 shows the K^+K^- invariant mass distribution of the $\phi(1020) \to K^+K^-$ candidates in the inclusive muon sample, with an additional requirement on the transverse momentum of the kaon misidentified as a muon, $4.2 < p_T < 7.0$ GeV. We display separately the sum and the difference of the distributions for the $K \to \mu$ tracks with positive and negative charges, as done in the case of K_S candidates, and use these distributions to measure the asymmetry for $K \to \mu$ tracks. The $\phi(1020)$ signal is fitted with a double Gaussian and the background is parametrized by the threshold function

$$f_{\rm bkg}(M) = (M - 2M_K)^{p_0} \exp(p_1 M + p_2 M^2 + p_3 M^3). \tag{B4}$$

All the parameters describing the signal, except its normalization, are fixed in the fit of the difference of the invariant mass distributions to the values obtained from the fit to the sum of the distributions.

5. Reconstruction of Λ baryons

The selection of $\Lambda \to p\pi^-$ decays [13] follows that of $K_S \to \pi^+\pi^-$, except that one of the tracks is assigned the mass of the proton. Figure 27 shows the $p\pi^-$ invariant mass distribution of $\Lambda \to p\pi^-$ candidates in the inclusive muon sample, with an additional requirement on the transverse momentum of the proton misidentified as a muon, for $4.2 < p_T < 7.0$ GeV. Also in this case we display separately the distributions for the sum and the difference of the distributions for Λ and $\bar{\Lambda}$ decays, and use them to determine the asymmetry for $p \to \mu$ tracks. The Λ baryon signal is fitted with a Gaussian, while the background is parametrized by a fourth (second) degree polynomial for the sum (difference) of the invariant mass distributions. All parameters describing the signal, except its normalization, are fixed in the fit of the difference of the invariant mass distributions to the values obtained from the fit to the sum of the distributions.

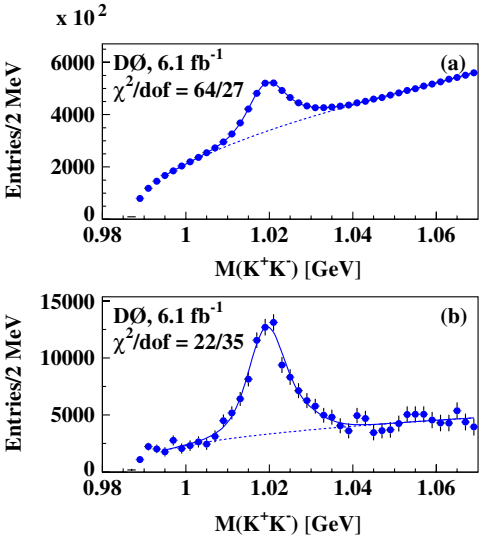

FIG. 26 (color online). The K^+K^- invariant mass distribution of $\phi(1020)$ candidates in the inclusive muon sample for $K \to \mu$ with $4.2 < p_T < 7.0$ GeV. (a) The sum of distributions of positive and negative $K \to \mu$ tracks and (b) their difference. The solid lines present the result of the fit and the dashed lines show the background contribution.

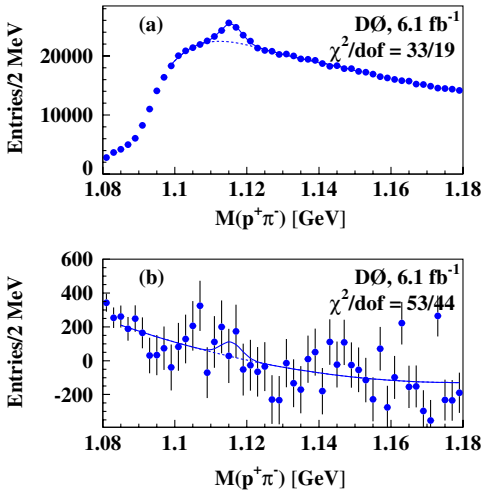

FIG. 27 (color online). The $p\pi^-$ invariant mass distribution of Λ candidates in the inclusive muon sample for $p \to \mu$ with $4.2 < p_T < 7.0$ GeV. (a) The sum of distributions of positive and negative $p \to \mu$ tracks and (b) their difference. The solid lines present the result of the fit and the dashed lines show the background contribution.

APPENDIX C: TRACK RECONSTRUCTION ASYMMETRY

In this measurement of $A_{\rm sl}^b$, we assume that the charge asymmetry of track reconstruction cancels as a result of the regular reversal of the magnets polarity. The method developed in Secs. V and XI provides a way of evaluating this assumption in data by comparing the track charge asymmetry $a_{\rm track}$ with that expected from already analyzed sources. We select events with one reconstructed muon and at least one additional track satisfying the selection criteria of Sec. III. The muon is not used in this study, but is required since the events are collected with single muon triggers. Nevertheless, the charges of the muon and the additional track can be correlated, and the asymmetry of the inclusive muon events can bias the observed track asymmetry. To eliminate this bias, we consider separately events in which the muon and the track have equal and opposite charges. The asymmetries in these samples can be expressed as

$$a_{\rm opp} = a_{\rm track} - a, \qquad a_{\rm equal} = a_{\rm track} + a. \tag{C1}$$

The asymmetry a is defined in Eq. (6), and the asymmetries $a_{\rm opp}$ and $a_{\rm equal}$ are computed as

$$a_{\rm opp} = \frac{n^{+-} - n^{-+}}{n^{+-} + n^{-+}}, \qquad a_{\rm equal} = \frac{n^{++} - n^{--}}{n^{++} + n^{--}}, \quad \text{(C2)}$$

where n^{ij} is the number of events containing a track with charge i and a muon with charge j. The track asymmetry $a_{\rm track}$ is computed as

$$a_{\rm track} = \tfrac{1}{2}(a_{\rm opp} + a_{\rm equal}). \quad \text{(C3)}$$

As discussed in Sec. XI, we expect the value of $a_{\rm track}$ to contain a contribution from the asymmetry of kaon reconstruction, even after averaging over the different magnet polarities. The expected value of $a_{\rm track}$ is therefore given by

$$a_{\rm track} = a_K^{\rm track} f_K^{\rm track}, \quad \text{(C4)}$$

where $f_K^{\rm track}$ is the fraction of reconstructed tracks that are kaons, and $a_K^{\rm track}$ is the charge asymmetry of kaon reconstruction.

The fraction $f_K^{\rm track}$ is measured using $K^{*0} \to K^+\pi^-$ decays [13]. The selected charged particle is assigned the kaon mass and combined with an additional track to produce the K^{*0} candidate. The K^{*0} selection and fitting procedure is described in Appendix B. The measured number of K^{*0} mesons is converted into the number of kaons using a method similar to that presented in Sec. V. The measured $f_K^{\rm track}$ fraction is assigned a systematic uncertainty as in Sec. VIII.

The same $K^{*0} \to K^+\pi^-$ decay is used to measure the kaon reconstruction asymmetry. This measurement can be biased by the asymmetry of the muon, because the charge of the kaon and the muon can be correlated. The kaon asymmetry is therefore measured separately in the samples in which the muon and the kaon have equal or opposite charges. The asymmetry $a_K^{\rm track}$ is computed in a way similar to Eq. (C3):

$$a_K^{\rm track} = \tfrac{1}{2}(a_K^{\rm opp} + a_K^{\rm equal}). \quad \text{(C5)}$$

The K^{*0} mass distribution is plotted separately for positive and negative kaons in each sample, and the sum and the difference of these distributions is fitted to extract the quantity Δ, corresponding to the difference in the number of K^{*0} decays with positive and negative kaons, and the quantity Σ, corresponding to their sum. The asymmetry $a_K^{\rm opp}$ is measured as $a_K^{\rm opp} = \Delta_{\rm opp}/\Sigma_{\rm opp}$, and a similar relation is used to obtain the asymmetry $a_K^{\rm equal}$.

The expected and observed track reconstruction asymmetry, i.e., the right and left sides of Eq. (C4), are compared in Fig. 28 as a function of track p_T. There is excellent agreement between these two quantities. The χ^2/d.o.f. for their difference is 5.4/5. The fit of $\delta_{\rm track} = a_{\rm track} - a_K^{\rm track} f_K^{\rm track}$ to a constant yields the following estimate for a residual track asymmetry of

$$\delta_{\rm track} = +0.000\,11 \pm 0.000\,35. \quad \text{(C6)}$$

We conclude that the residual track asymmetry is consistent with zero as expected. The uncertainty on this value is about a factor of 16 times smaller than the observed charge asymmetry in the like-sign dimuon events. This study provides an additional confirmation of the validity of the method used in this analysis.

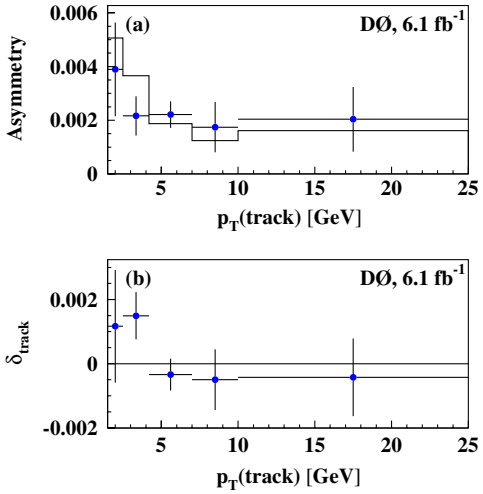

FIG. 28 (color online). (a) The expected (points with errors) and measured (histogram with negligible uncertainties) track reconstruction asymmetry. (b) The quantity $\delta_{\rm track} = a_{\rm track} - a_K^{\rm track} f_K^{\rm track}$.

APPENDIX D: TRIGGER ASYMMETRY

We determine the kaon, pion, and proton charge asymmetries using events passing at least one single muon trigger, and we apply the same asymmetries to the like-sign dimuon events collected with dimuon triggers. Similarly, we measure the muon reconstruction asymmetry using events passing the dimuon triggers, and we use the same quantity for events collected with the single muon triggers. If the trigger selection is charge asymmetric, and this asymmetry is different for single muon and for dimuon triggers, the obtained value of $A_{\rm sl}^b$ can be biased. Since we extract the asymmetry $A_{\rm sl}^b$ from the difference $A - \alpha a$, and because the value of α is very close to unity, our measurement is especially sensitive to a difference between the charge asymmetry of dimuon and single muon triggers.

To examine the impact of this difference on our result, we repeat the measurement of $A_{\rm sl}^b$ using dimuon events passing any single muon trigger without requiring dimuon triggers. The result of this test, given in column O of Table XVI, does not indicate a bias from the trigger selection. In addition, we measure $A_{\rm sl}^b$ using dimuon events passing both single muon and dimuon triggers. The result of this test is given in column P of Table XVI. These two tests provide a residual difference δ_T between the asymmetry of dimuon triggers and single muon triggers of

$$\delta_T = +0.000\,10 \pm 0.000\,29. \quad \text{(D1)}$$

From this result, we conclude that the trigger selections do not produce any significant bias to the value of $A_{\rm sl}^b$.

TABLE XVII. Values of $\alpha_i \equiv F_K^i/f_K^i$ obtained through two methods, with their statistical uncertainties.

Bin	α_i from Table III	α_i from null fit
0	1.309 ± 0.340	0.954 ± 0.217
1	0.987 ± 0.082	0.942 ± 0.069
2	1.022 ± 0.050	1.031 ± 0.027
3	0.758 ± 0.101	0.806 ± 0.055
4	1.406 ± 0.159	1.292 ± 0.079
All	0.998 ± 0.038	0.990 ± 0.022

APPENDIX E: ALTERNATIVE MEASUREMENT OF F_K/f_K

We consider two methods to obtain the parameters $\alpha_i \equiv F_K^i/f_K^i$ in the p_T interval i from

$$\alpha_i = 2\frac{N_i(K^{*0} \to K \to \mu)}{N_i}\frac{n_i}{n_i(K^{*0} \to K \to \mu)}, \quad \text{(E1)}$$

where N_i refers to the like-sign dimuon sample and n_i refers to the inclusive muon sample. $N_i(K^{*0} \to K \to \mu)$ and $n_i(K^{*0} \to K \to \mu)$ are obtained by fitting the invariant mass histograms of $K^{*0} \to \pi K \to \mu$ in the like-sign dimuon and inclusive muon samples, respectively. These fits require precise modeling of the ρ^0 resonance and of other backgrounds. In the first method we use the results listed in Table III and obtain the values of α_i listed in Table XVII.

A second set of values for the α_i parameters can be obtained by finding a scale factor which minimizes the differences between invariant mass distributions for the K^{*0} candidates in the inclusive muon and dimuon samples (null fit method). Invariant mass distributions for K^{*0} candidates analogous to the ones shown in Fig. 22 and 23 are built for each bin of $K \to \mu$ transverse momentum. We scale the invariant mass distribution in the inclusive muon sample by a factor $\alpha_i N_i/(2n_i)$ and subtract it from the invariant mass distribution obtained from the dimuon sample. The contributions from the ρ resonance and from other backgrounds cancel to first order in the difference of the two invariant mass distributions, simplifying the convergence of mass fits. We then vary the factor α_i and find the value that yields a null normalization factor for the residual K^{*0} signal. The statistical uncertainty on α_i is obtained by choosing the value of the scale factor which yields a positive (negative) value of this normalization factor which is equal to its uncertainty. The values of α_i obtained with this method are also listed in Table XVII, with their statistical uncertainties. There is remarkable agreement between the values of α_i obtained using the two methods.

[1] A. Lenz and U. Nierste, J. High Energy Phys. 06 (2007) 072.
[2] C. Amsler *et al.*, Phys. Lett. B **667**, 1 (2008), and 2009 partial update for the 2010 edition.
[3] A. D. Sakharov, Pis'ma Zh. Eksp. Teor. Fiz. **5**, 32 (1967) [JETP Lett. **5**, 24 (1967)], Sov. Phys. Usp. **34**, 392 (1991).
[4] M. B. Gavela *et al.*, Mod. Phys. Lett. A **9**, 795 (1994); Nucl. Phys. **B430**, 382 (1994); P. Huet and E. Sather, Phys. Rev. D **51**, 379 (1995).
[5] B. Aubert *et al.* (*BABAR* Collaboration), Phys. Rev. Lett. **96**, 251802 (2006); arXiv:hep-ex/0607091.
[6] E. Nakano *et al.* (Belle Collaboration), Phys. Rev. D **73**, 112002 (2006).
[7] L. Randall and S. Su, Nucl. Phys. **B540**, 37 (1999).
[8] J. L. Hewett, arXiv:hep-ph/9803370.
[9] G. W. S. Hou, arXiv:0810.3396.
[10] A. Soni *et al.*, Phys. Lett. B **683**, 302 (2010); arXiv:1002.0595 [Phys. Rev. D (to be published)] and references therein.
[11] M. Blanke *et al.*, J. High Energy Phys. 12 (2006) 003; W. Altmannshofer *et al.*, Nucl. Phys. **B830**, 17 (2010).
[12] Y. Grossman *et al.*, Phys. Rev. Lett. **97**, 151801 (2006).
[13] Charge conjugation invariance is implied throughout this article.
[14] V. M. Abazov *et al.*, Nucl. Instrum. Methods Phys. Res., Sect. A **552**, 372 (2005).
[15] V. M. Abazov *et al.* (D0 Collaboration), Nucl. Instrum. Methods Phys. Res., Sect. A **565**, 463 (2006).
[16] S. N. Ahmed *et al.*, arXiv:1005.0801 [Nucl. Instrum. Methods Phys. Res. Sect. A (to be published)]; R. Angstadt *et al.*, arXiv:0911.2522.
[17] V. M. Abazov *et al.* (D0 Collaboration), Phys. Rev. D **74**, 092001 (2006).
[18] Pseudorapidity $\eta \equiv -\ln[\tan(\theta/2)]$, where θ is the polar angle of the track relative to the direction of the proton beam; ϕ is the azimuthal angle with respect to the proton beam, and $\phi = 90°$ is defined as the vertical axis.
[19] T. Sjöstrand *et al.*, Comput. Phys. Commun. **135**, 238 (2001).
[20] D. G. Lange, Nucl. Instrum. Methods Phys. Res., Sect. A **462**, 152 (2001); for details see http://www.slac.stanford.edu/~lange/EvtGen.
[21] J. Pumplin *et al.*, J. High Energy Phys. 02 (2006) 032.
[22] R. Brun and F. Carminati, CERN program library long writeup W5013 (unpublished).
[23] V. M. Abazov *et al.* (D0 Collaboration), Phys. Rev. Lett. **100**, 211802 (2008).
[24] E. Barberio *et al.* (HFAG Collaboration), arXiv:0808.1297.
[25] V. M. Abazov *et al.* (D0 Collaboration), arXiv:0904.3907 [Phys. Rev. D (to be published)].
[26] V. M. Abazov *et al.* (D0 Collaboration), Phys. Rev. Lett.

101, 241801 (2008); **98**, 121801 (2007).
[27] T. Aaltonen *et al.* (CDF Collaboration), Phys. Rev. Lett. **100**, 161802 (2008).
[28] CDF/D0 $\Delta\Gamma_s$, β_s Combination Working Group, D0 Note 5928-CONF, 2009, and CDF Public Note CDF/ANAL/BOTTOM/PUBLIC/9787, 2009.
[29] G. C. Branco, L. Lavoura, and J. P. Silva, *CP Violation* (Clarendon, Oxford, 1999).